

The JCMT Nearby Galaxies Legacy Survey – X. Environmental Effects on the Molecular Gas and Star Formation Properties of Spiral Galaxies

Angus Mok¹, C. D. Wilson¹, J. Golding¹, B. E. Warren², F. P. Israel³, S. Serjeant⁴, J. H. Knapen^{5,6}, J. R. Sánchez-Gallego^{5,6,7}, P. Barmby⁸, G. J. Bendo⁹, E. Rosolowsky¹⁰, and P. van der Werf¹¹

¹ Department of Physics & Astronomy, McMaster University, Hamilton, Ontario L8S 4M1, Canada

² International Centre for Radio Astronomy Research, M468, University of Western Australia, 35 Stirling Hwy, Crawley, WA 6009, Australia

³ Sterrewacht Leiden, Leiden University, PO Box 9513, 2300 RA Leiden, The Netherlands

⁴ Department of Physics & Astronomy, The Open University, Milton Keynes MK7 6AA, United Kingdom

⁵ Instituto de Astrofísica de Canarias, E-38205 La Laguna, Tenerife, Spain

⁶ Departamento de Astrofísica, Universidad de La Laguna, E-38200 La Laguna, Tenerife, Spain

⁷ Department of Physics and Astronomy, University of Kentucky, 40506-0055, Lexington, Kentucky, United States

⁸ Department of Physics & Astronomy, University of Western Ontario, London, Ontario N6A 3K7, Canada

⁹ UK ALMA Regional Centre Node, Jodrell Bank Centre for Astrophysics, School of Physics and Astronomy, University of Manchester, Oxford Road, Manchester M13 9PL, United Kingdom

¹⁰ Department of Physics, University of Alberta, Edmonton, Ontario T6G 2R3, Canada

¹¹ Kapteyn Astronomical Institute, Postbus 800, NL-9700 AV Groningen, The Netherlands

13 June 2021

ABSTRACT

We present a study of the molecular gas properties in a sample of 98 H I - flux selected spiral galaxies within ~ 25 Mpc, using the CO $J = 3 - 2$ line observed with the James Clerk Maxwell Telescope. We use the technique of survival analysis to incorporate galaxies with CO upper limits into our results. Comparing the group and Virgo samples, we find a larger mean H₂ mass in the Virgo galaxies, despite their lower mean H I mass. This leads to a significantly higher H₂ to H I ratio for Virgo galaxies. Combining our data with complementary H α star formation rate measurements, Virgo galaxies have longer molecular gas depletion times compared to group galaxies, due to their higher H₂ masses and lower star formation rates. We suggest that the longer depletion times may be a result of heating processes in the cluster environment or differences in the turbulent pressure. From the full sample, we find that the molecular gas depletion time has a positive correlation with the stellar mass, indicative of differences in the star formation process between low and high mass galaxies, and a negative correlation between the molecular gas depletion time and the specific star formation rate.

Key words: galaxies: ISM – galaxies: spiral – ISM: molecules – stars: formation

1 INTRODUCTION

Star formation in the Universe takes place inside galaxies, where they convert their available gas reservoirs into stars. In particular, stars are born inside cold, dense molecular clouds and so a complete analysis of the star formation process requires the study of a galaxy’s molecular gas content. Previous work has shown that star formation is more closely linked to the molecular gas, as compared to either the atomic hydrogen (H I) mass or the total gas (H I + H₂) mass (Bigiel et al. 2008; Leroy et al. 2008). These studies of star formation and molecular gas data for nearby galaxies have also revealed short H₂ depletion times compared to the age of the galaxy

(Leroy et al. 2008; Saintonge et al. 2011; Bigiel et al. 2011), which suggests an ongoing need to replenish their molecular gas reservoir.

Spiral galaxies are the primary targets for this type of analysis, as star formation does not take place equally in all galaxies. For example, the morphological classification between early- and late-type galaxies tends to correspond to their stellar population, such as the well-known ‘red sequence’ and ‘blue cloud’ found in colour-magnitude diagrams (e.g. Strateva et al. 2001; Bell et al. 2003). The key difference between these two galaxy populations is their typical star formation state: whether they are undergoing active star formation or if they are mostly quiescent objects. Even for spiral galaxies

along the Hubble sequence, the star formation rate has been shown to differ greatly (Kennicutt 1998a).

The local environment of these galaxies can also influence galaxy evolution, from isolated galaxies, to groups of tens of galaxies, to clusters of thousands of galaxies. Denser environments in the Universe are dominated by early-type, red sequence galaxies (Baldry et al. 2006; Blanton & Moustakas 2009). For spiral galaxies inside clusters, observations have shown a deficiency of atomic hydrogen (Chamaraux et al. 1980; Haynes & Giovanelli 1986; Solanes et al. 2001; Gavazzi et al. 2005) and a reduction in the scale length of $H\alpha$ emission (Koopmann et al. 2006), which is linked to young stars and star formation. On a smaller scale, some studies of galaxies with nearby companions have shown that star formation is generally unaffected, other than for the rare cases where mergers and interactions leads to a statistically significant but moderate enhancement in the star formation rate (Knapen & James 2009; Knapen et al. 2015). On the other hand, a larger sample of interacting pairs from the SDSS shows signs of a star formation enhancement at the smallest separations (Ellison et al. 2013).

Many possible physical processes have been invoked to explain the effects of environment. For example, galaxies may be affected by harassment from other cluster members (Moore et al. 1996) or be starved from their gas supply (Larson et al. 1980). In more extreme environments, ram-pressure stripping of a galaxy’s gas content can take place (Gunn & Gott 1972), and interactions and mergers can directly increase the gas content of galaxies or change the distribution of their gas. However, it remains unclear whether these processes can directly affect the molecular gas content, with its high surface density and its location deep inside the galaxy’s potential well.

A good place to study the effects of environment on galaxy evolution is the Virgo Cluster, due to its close proximity and the large numbers of infalling spiral galaxies. One of the initial studies of molecular gas in Virgo spirals using the CO tracer was performed with the 7 metre Bell Laboratories antenna (Stark et al. 1986), finding correlations between the radio continuum and far-infrared data. Further studies helped determine the conversion ratio between the CO $J = 1 - 0$ luminosity and the molecular gas mass (Knapp et al. 1987). Subsequent CO observations with the Five College Radio Astronomy Observatory (FCRAO) have shown that the molecular content of Virgo spirals may be quite similar to that of field galaxies (Kenney & Young 1989), but other groups have found hints of a reduction in the size of the molecular gas disk in Virgo spirals (Fumagalli & Gavazzi 2008). Recent results from the HeViCS survey indicate a reduction in the amount of molecular gas per unit stellar mass in H I deficient galaxies (Corbelli et al. 2012). Finally, Vollmer et al. (2012) have looked at resolved measurements of 12 Virgo spiral galaxies and found a relationship between molecular gas mass and star formation, but no evidence for environmental differences in the star formation efficiency. A complete picture of the effects of environment on star formation and the molecular gas content of galaxies remains elusive.

This paper uses a large sample of 98 H I - flux selected spiral galaxies, with a majority coming from the original Nearby Galaxies Legacy Survey (Wilson et al. 2012). One of the main objectives of the NGLS is to study the effect of environment on a galaxy’s molecular gas content by using CO $J = 3 - 2$ observations with the James Clerk Maxwell Telescope (JCMT) (Wilson et al. 2009, 2012). The CO $J = 3 - 2$ line is a tracer for warmer and denser gas than the CO $J = 1 - 0$ line and appears to be well correlated with the far-infrared luminosity, a proxy for the star formation rate (Iono et al. 2009; Wilson et al. 2012). We supplement the NGLS data with

follow up JCMT surveys in the Virgo cluster and some galaxies from the Herschel Reference Survey (HRS) sample. Our analysis also includes data from other sources, including stellar masses and star formation rates.

In § 2, we present our observations and the general properties of our sample. In § 3, we discuss the use of survival analysis for datasets containing censored data (such as the H_2 gas mass) and present our analysis of galaxy properties. We also include a detailed comparison of the group and Virgo populations, as well as the CO detected and non-detected samples. In § 4, we present some specific tests of our results and the correlations found between various properties of the galaxies in our sample.

2 SAMPLE SELECTION, OBSERVATIONS, AND DATA PROCESSING

2.1 Sample Selection

The objective of our analysis is to create a large sample of nearby, gas-rich spiral galaxies. First, we select only spiral galaxies with H I flux $> 6.3 \text{ Jy km s}^{-1}$, which corresponds to a log H I mass of 8.61 (in solar units) at the sample’s median distance of 16.7 Mpc. The H I flux is identified using the HyperLeda database (Patrel et al. 2003; Makarov et al. 2014), which compiles different survey results and produces a weighted average of the results. The database can be found online¹. We also use the HyperLeda database to select only spiral galaxies using the morphological type code, removing from the sample galaxies that are ellipticals or lenticulars. We identify Virgo galaxies in our sample using the catalog from Binggeli et al. (1985).

Next, we impose a size limit on our galaxies. The non-Virgo sample is limited to galaxies with $D_{25} < 5'$, which at our distance limit of ~ 25 Mpc corresponds to $D_{25} < 36$ kpc. We therefore include only the 39 Virgo spiral galaxies with $D_{25} < 7.4'$ in order to match the physical size limits of of the Virgo and non-Virgo samples. Note that for all galaxies in the Virgo sample, we have assumed a standard distance of 16.7 Mpc (Mei et al. 2007).

To subdivide our sample further, we use the Garcia (1993) catalog. They used the LEDA data base to identify a robust set of 485 groups out of a sample of 6392 local galaxies by their 3D projection in space. Comparing our galaxy sample to the groups from their catalog yields a total of 40 galaxies. In addition, we place two galaxies, NGC0450 and NGC2146A, which are known from the Karachentsev (1972) catalog to be in close pairs, into this category as well. This results in a total of 42 spiral galaxies meeting our H I flux and size criterion that are members of groups. The 17 remaining galaxies constitute our field (or non-group) galaxy sample.

A summary of the sample sources, subdivided into the field, group, and Virgo populations, are presented in Table 1. There are three main sources of the CO $J = 3 - 2$ data. The first is the Nearby Galaxies Legacy Survey (Wilson et al. 2012). The second is a follow on study to complete observations in the Virgo cluster (project code M09AC05), using the same criterion as the parent NGLS survey. As a result, we do not expect significant differences between these two sources. Finally, to increase the number of galaxies in our sample, we also include a subset of Herschel Reference Survey (HRS) galaxies that fulfill the criteria listed above and are not already a member of the NGLS (Boselli et al. 2010). One potential difference between the three sources of data is that the Herschel

¹ <http://leda.univ-lyon1.fr/>

Table 1. Sample Sources

Category	Total	Field	Group	Virgo
NGLS	53	12	21	20
Virgo Follow-Up (M09AC05)	17	0	0	17
HRS (M14AC03)	28	5	21	2
Total	98	17	42	39

Reference Survey also has a K-band (or stellar mass) selection, but we do not expect it to greatly influence the results in this paper. Also, a subset of group galaxies is identified by the HRS as being in the Virgo outskirts, which we have kept in the group category given their local environment is likely more similar to the group than Virgo category. A full discussion of the three sources of our CO $J = 3 - 2$ can be found in Appendix A.

Finally, due to our sample criteria, we are biased towards gas-rich, nearby, moderately-sized galaxies and to the detriment of H I deficient, far-away, larger, non-spiral galaxies. This is done to ensure a consistent statistical sample and to obtain satisfactory detection rates, as discussed in the observation section below.

2.2 Observations

The observations and data processing for the 155 galaxies in the NGLS are described in detail in Wilson et al. (2012), and so only a basic summary is given here. We observed the CO $J = 3 - 2$ line with the JCMT’s HARP instrument (Buckle et al. 2009), which has $\eta_{MB} = 0.6$ and an angular resolution of $14.5''$. All galaxies were mapped out to at least $D_{25}/2$ with a 1 sigma sensitivity of better than 19 mK (T_A^* ; 32 mK T_{MB}) at a spectral resolution of 20 km s^{-1} . The CO luminosities are measured on the T_{MB} scale. The internal calibration uncertainty is 10%. The reduced images, noise maps, and spectral cubes are available via the survey website² and also via the Canadian Astronomical Data Centre³.

For galaxies with CO detections, we used the zeroth moment maps made with a noise cutoff of 2σ to measure the CO $J = 3 - 2$ luminosity (see Wilson et al. (2012) for further details). We use an aperture chosen by eye to capture all of the real emission from the galaxy. For galaxies without detections, 2σ upper limits were calculated from the noise maps assuming a line width of 100 km s^{-1} and using an aperture with a diameter of $1'$. The full sample includes 57 spiral galaxies from the NGLS, 14 spiral galaxies observed with the JCMT in 2009 February-May (JCMT program M09AC05), and 27 spiral galaxies from the Herschel Reference Survey (JCMT program M14AC03). The galaxies were processed using the same methods adopted for the NGLS and the calibration uncertainty for these data is also 10%.

We convert the CO $J = 3 - 2$ luminosities to molecular hydrogen mass adopting a CO-to- H_2 conversion factor of $X_{CO} = 2 \times 10^{20} \text{ cm}^{-2} (\text{K km s}^{-1})^{-1}$ (Strong et al. 1988) and a CO $J = 3 - 2/J = 1 - 0$ line ratio of 0.18 (Wilson et al. 2012). This measurement is similar to the CO $J = 3 - 2/J = 1 - 0$ line ratio of Virgo spiral galaxies obtained by other groups (Hafok & Stutzki 2003). With these assumptions, the molecular hydrogen mass is given by:

$$M_{H_2} = 17.8(R_{31}/0.18)^{-1} L_{CO(3-2)} \quad (1)$$

where R_{31} is the CO $J = 3 - 2/J = 1 - 0$ line ratio, M_{H_2} is in M_\odot , and $L_{CO(3-2)}$ is in units of K km $s^{-1} \text{ pc}^2$.

We note that the assumption of a constant conversion factor may not be correct in all cases. For example, the conversion factor can be affected by the ambient radiation field and the metallicity (Israel 1997). Adopting a single value for X_{CO} will produce an underestimate of the molecular gas mass in galaxies where the metallicity is more than about a factor of two below solar (Wilson 1995; Arimoto et al. 1996; Bolatto et al. 2008; Leroy et al. 2012). In a recent review paper on the conversion factor, Bolatto et al. (2013) suggested a possible prescription that is based on the gas surface density and metallicity. However, given the large scatter in their observational results and the fact that our galaxies are all relatively ‘normal’ spiral galaxies, we have decided to maintain the constant conversion factor used in the previous papers in this series.

We also use data sourced from other surveys. As stated in the section on our sample selections, the H I fluxes and morphological types for all the galaxies are taken from the most recent values of the HyperLeda database. We also use the database for measurements of redshift distances and D_{25} sizes. Stellar masses for individual galaxies are taken from the S⁴G survey (Sheth et al. 2010) using the NASA/IPAC Infrared Science Archive, for all the galaxies where they are available. The S⁴G survey have calibrated their stellar masses using the two IRAC bands, 3.6 and 4.5 μm , using the prescription from Eskew et al. (2012) and assuming a Salpeter IMF. To convert to a Kroupa IMF, we multiply by a factor of 0.7, which has been used in previous work (e.g. Elbaz et al. 2007). We have also used the distance measurements in the S⁴G catalog to adjust the stellar masses to correspond to the distances used in this analysis.

For the 8 galaxies where the stellar mass is unavailable, we substitute K-band luminosities from the 2MASS database using the extended source catalogue (Skrutskie et al. 2006). We have assumed a total mass-to-light ratio of 0.533 in solar units for Sbc/Sc-type spiral galaxies from Table 7 in Portinari et al. (2004) with the Kroupa IMF, as they comprise a majority of the galaxies without masses from the S⁴G survey. For comparison, the corresponding value for Sa/Sab-type spiral galaxies is 0.698. The average stellar mass for these galaxies is lower than that of the sample as a whole, but since they only comprise a small percentage of the total sample, we do not expect this difference to have a significant effect on our results.

In addition, H α -derived star formation rates are taken from Sánchez-Gallego et al. (2012), with typical uncertainties of 18 per cent. We note that the formulas from Kennicutt et al. (2009) assume a stellar initial mass function (IMF) from Kroupa & Weidner (2003). For the additional spiral galaxies from the Virgo cluster observed in the M09AC05 program, we use H α fluxes from the GOLDmine database (Gavazzi et al. 2003). For the galaxies from the HRS sample, we use the data from a new H α study of these galaxies (Boselli et al. 2015). The H α data from all three sources are corrected for extinction and converted into star formation rates using the same procedure as Sánchez-Gallego et al. (2012). We also investigate the effects of including a mid-IR star formation tracer using data from the S⁴G survey and find there is moderate scatter between the two measurements. However, we have chosen to present the extinction-corrected H α data in order to maintain continuity with the previous papers in this series.

Detailed properties for the individual galaxies are presented for the field galaxies in Table B1, the group galaxies in Table B2, and the Virgo sample in Table B3, located in Appendix B. Maps of the CO detected galaxies can be found in Appendix C. The field

² http://www.physics.mcmaster.ca/~wilson/www_xfer/NGLS/

³ DOI 10.1111/j.1365-2966.2012.21453.x

sample is shown in Figure C1, the group sample in Figures C2 and C3, and the Virgo sample in Figure C4. Virgo galaxies observed with two overlapping fields are presented in Figure C5, while NGC 4303, observed using the raster method, is presented in Figure C6. Note that images of NGC4254 and NGC4579 can be found in Wilson et al. (2012) and are not repeated here.

2.3 Survival Analysis and the Kaplan-Meier Estimator

In statistics, survival analysis is often used with censored datasets, i.e. datasets that include upper or lower limits. The original purpose of survival analysis is in medicine, where data censoring is important in clinical trials because patients can either die or potentially leave the trial. This procedure has subsequently been applied to datasets in other scientific fields, such as astronomy, where ‘deaths’ are replaced with measurements and patients who leave the trial are replaced with censored data, such as upper or lower limits (e.g. Young et al. 2011). This method of survival analysis allows us to determine statistical properties that are difficult to ascertain using classical methods when many of the measurements are censored.

For our sample of galaxies, we first use the Kaplan-Meier estimator to fit survival functions to our data. It is a non-parametric, maximum likelihood statistical estimator (Kaplan & Meier 1958). In this study, we used the statistical package called SURVIVAL, which is written in R and can be found at the standard R repository⁴. Once we have fit a survival function to our dataset, we can then determine the modified versions of important statistical quantities. For example, we can find the ‘median’ value of the dataset by finding the point where the survival function is equal to 0.5 and the ‘restricted mean’ of the dataset by integrating the survival function to the last detected point.

To differentiate between survival functions and determine if they are significantly different from one another, we have used the log-rank test. The log-rank test was first introduced in Mantel (1966) and is often used to compare the effectiveness of new treatments in clinical trials. In our paper, we have applied survival analysis to the H₂ mass and its other derived quantities, such as the molecular gas depletion time (the H₂ gas mass divided by the star formation rate) and the stellar mass normalized H₂ mass. The use of survival analysis and the log-rank test for these cases has the primary advantage of incorporating all the data collected, instead of discarding galaxies without CO detections. For non-censored datasets, we will use the standard Kolmogorov-Smirnov test for distinguishing between two distributions. An example of the application of the Kaplan-Meier estimator to the H₂ masses and the stellar mass normalized H₂ masses is presented in Figure 1, where the cumulative distribution functions are plotted.

The application of survival analysis to the total gas mass and its related quantities, such as the total gas depletion time (total gas mass divided by the star formation rate), presents one important difference compared to the H₂ gas mass alone. Since the galaxies without CO detections do have H I gas masses, it is not proper to treat galaxies without CO detections as pure upper limits for their total gas mass. Rather, they should be considered ‘interval censored’, where the true value is in between two values. In this case, the total gas mass for these galaxies would lie between their measured H I gas masses and the sum of their H I gas mass and the H₂ upper limit. For these datasets, we use the statistical package called

INTERVAL, which can be found at the standard R repository⁵. The package also includes an implementation of the log-rank test routine ICTEST for interval censored data. In order to be consistent, we also use this particular INTERVAL routine for our left and right censored data as well. For those cases, we substitute in appropriate interval limits, such as -99 or 99 for the log upper and lower limits.

3 RESULTS

3.1 Overview of Galaxy Properties in the Three Environments

The general properties of the galaxies in our sample, separated into field, group, and Virgo subsets, are presented in Table 2. The first three columns are mean H I mass, D_{25} sizes, and distances taken from the HyperLeda database, using velocities corrected for Virgo infall and assuming a cosmology of $H_o = 70 \text{ km s}^{-1} \text{ Mpc}^{-1}$, $\Omega_M = 0.27$, $\Omega_\Lambda = 0.73$. The next column is the CO detection rate for each individual sample, followed by the mean H₂ and H₂ + H I masses, with the calculations outlined in the previous section. Finally, we present the mean stellar mass for each of the samples.

The mean log H₂ mass, calculated from the Kaplan-Meier estimator of the survival function, is highest in the Virgo sample, followed by the field and group samples. The log-rank test on the group and Virgo samples shows a p-value of 0.0279, which suggests that there is a difference in the H₂ mass distributions between the two populations, when we take into account the censored data. For the case of atomic hydrogen, the mean H I mass is lowest for the Virgo galaxies, followed by the group and field samples. Relative H I deficiency of Virgo galaxies has been reported in previous studies of Virgo galaxies (e.g. Chamaraux et al. 1980; Haynes & Giovanelli 1986; Solanes et al. 2001; Gavazzi et al. 2005), so it is not surprising to see this difference in our sample, even when we have selected based on a H I flux limit. The Kolmogorov-Smirnov test, performed for datasets that do not contain censored data, shows that the H I masses of the Virgo and group galaxies are not drawn from the same distribution, with a p-value of 4×10^{-4} .

The Virgo galaxies are all at the same assumed distance of 16.7 Mpc, while the group and field samples have larger mean distances. As a result, the Kolmogorov-Smirnov test reveals that the distribution in the distances of Virgo galaxies can be distinguished from both field and the group galaxies. Replacing the constant 16.7 Mpc with a Gaussian distributed sample with reasonable scatter does not change this result. Although the mean log total gas mass (H I + H₂) is slightly higher for the field galaxies, followed by the group, and Virgo samples, the difference is not statistically significant. The stellar masses of the Virgo and group samples are also quite similar, while the field galaxies have a lower mean value. The Kolmogorov-Smirnov test shows that the stellar mass distributions of the group and Virgo samples cannot be distinguished ($p = 0.4031$).

3.2 Group/Virgo Comparison

In Table 3, we present a summary of the properties of the group/Virgo, CO detected/CO non-detected samples, and a test case comparing the group and Virgo samples using CO detected galaxies only. In Table 4, we present the results from performing the

⁴ <http://cran.r-project.org/web/packages/survival/index.html>

⁵ <http://cran.r-project.org/web/packages/interval/index.html>

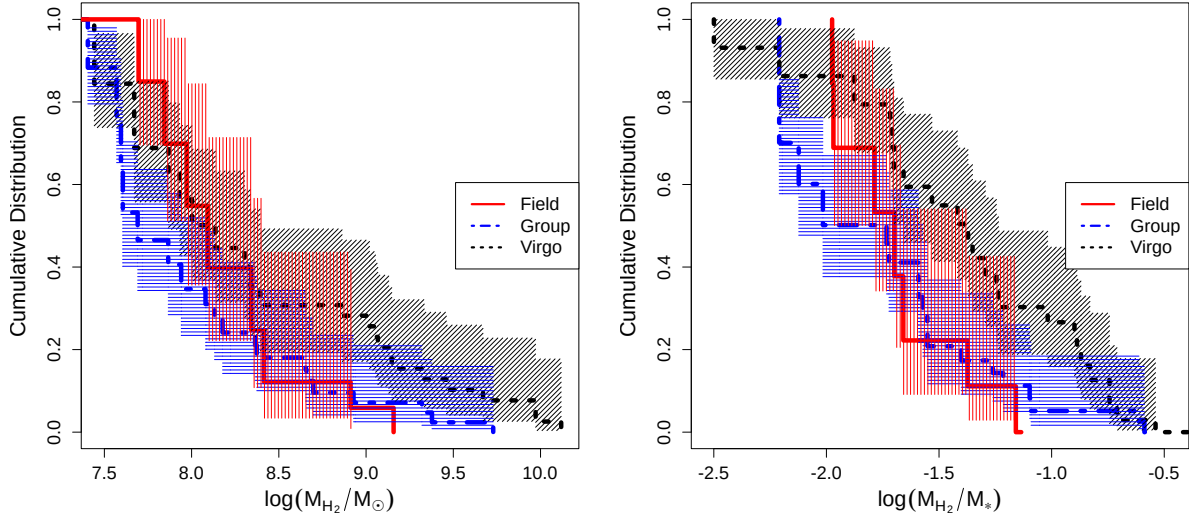


Figure 1. **Left:** Survival functions for the molecular hydrogen gas mass in the field (red solid line), group (blue dot-dash line), and Virgo (black dashed line) sample galaxies using the Kaplan-Meier estimator. The ‘steps’ in the distribution correspond to detections. The 95% confidence intervals are overlaid for the three distributions. **Right:** Survival functions for the molecular hydrogen gas mass divided by the stellar mass in the field, group and Virgo sample galaxies.

Table 2. Galaxy Properties as a Function of Environment

Type (# of galaxies)	$\bar{\log} M_{HI}^{-1}$ (M_{\odot})	\bar{D}_{25}^{-1} (kpc)	$\bar{\text{Distance}}^{-1}$ (Mpc)	CO detection rate ² (%)	$\bar{\log} M_{H_2}^{-3}$ (M_{\odot})	$\bar{\log} M_{H_2+HI}^{-3}$ (M_{\odot})	$\bar{\log} M_{*}^{-1}$ (M_{\odot})
Field (17)	9.23 ± 0.07	16.1 ± 1.8	20.1 ± 0.8	35 ± 9	8.17 ± 0.07	9.30 ± 0.06	9.58 ± 0.14
Group (42)	9.17 ± 0.04	13.1 ± 0.8	18.6 ± 0.7	40 ± 6	7.98 ± 0.08	9.24 ± 0.04	9.65 ± 0.07
Virgo (39)	8.99 ± 0.05	18.6 ± 2.0	16.7	54 ± 9	8.34 ± 0.13	9.17 ± 0.06	9.65 ± 0.11
CO Detected (44)	9.15 ± 0.05	19.9 ± 1.7	17.5 ± 0.5	100	8.61 ± 0.11	9.35 ± 0.05	9.97 ± 0.06
CO Non-Detected (54)	9.07 ± 0.04	12.5 ± 0.8	18.6 ± 0.5	0	$(8.28 \pm 0.06)^4$	$(9.16 \pm 0.03)^4$	9.36 ± 0.07

¹ Standard error of the means

² Binomial confidence intervals

³ Restricted mean and standard errors from the Kaplan-Meier estimator of the survival functions

⁴ Mean of the 2σ upper limits for the CO Non-Detected sample

Table 3. Selected Properties of the Group, Virgo, CO Detected, and CO Non-Detected Populations

Mean Quantity	Group (42)	Virgo (39)	CO Detected (44)	CO Non-Detected (54)
$\log M_{HI} [M_{\odot}]$	9.17 ± 0.04	8.99 ± 0.05	9.15 ± 0.05	9.07 ± 0.04
$\log M_{H_2} [M_{\odot}]^1$	7.98 ± 0.08	8.34 ± 0.13	8.61 ± 0.01	$(8.28 \pm 0.06)^2$
$\log M_{*} [M_{\odot}]$	9.65 ± 0.07	9.65 ± 0.11	9.97 ± 0.06	9.36 ± 0.07
$\log M_{H_2+HI} [M_{\odot}]^1$	9.24 ± 0.04	9.17 ± 0.06	9.35 ± 0.05	$(9.16 \pm 0.03)^2$
M_{H_2}/M_{HI}^1	0.23 ± 0.09	0.75 ± 0.20	0.87 ± 0.19	$(0.26 \pm 0.03)^2$
M_{H_2}/M_{*}^1	0.033 ± 0.008	0.068 ± 0.010	0.07 ± 0.01	$(0.26 \pm 0.07)^2$
M_{HI}/M_{*}	0.52 ± 0.11	0.50 ± 0.12	0.22 ± 0.03	0.82 ± 0.12
M_{H_2+HI}/M_{*}^1	0.57 ± 0.12	0.63 ± 0.14	0.29 ± 0.03	$(1.08 \pm 0.18)^2$
$\log \text{SFR} [M_{\odot} \text{ yr}^{-1}]$	-0.49 ± 0.07	-0.69 ± 0.11	-0.35 ± 0.09	-0.72 ± 0.07
$\log \text{sSFR} [\text{yr}^{-1}]$	-10.14 ± 0.06	-10.34 ± 0.06	-10.32 ± 0.06	-10.08 ± 0.06
$\log M_{H_2}/\text{SFR} [\text{yr}]^1$	8.44 ± 0.07	8.97 ± 0.06	8.96 ± 0.08	$(9.00 \pm 0.08)^2$
$\log M_{HI}/\text{SFR} [\text{yr}]$	9.71 ± 0.07	9.67 ± 0.08	9.50 ± 0.07	9.79 ± 0.05
$\log M_{H_2+HI}/\text{SFR} [\text{yr}]^1$	9.73 ± 0.05	9.86 ± 0.07	9.70 ± 0.06	$(9.88 \pm 0.05)^2$

¹ Restricted mean and standard errors from the Kaplan-Meier estimator of the survival functions

² Mean of the 2σ upper limits for the CO Non-Detected sample

Table 4. Significance Tests Between Different Samples

Mean Quantity	Group/Virgo	Group/Virgo (CO Det. Only)	CO Det./ Non-Det.
$\log M_{HI} [M_{\odot}]$	4×10^{-4}	<u>0.0181</u>	0.7680
$\log M_{H_2} [M_{\odot}]$	<u>0.0279</u> ¹	0.1635	–
$\log M_{*} [M_{\odot}]$	0.6304	0.3090	1×10^{-9}
$\log M_{H_2+HI} [M_{\odot}]$	0.7720 ¹	0.3653	–
M_{H_2}/M_{HI}	0.0095 ¹	0.0786	–
M_{H_2}/M_{*}	<u>0.0272</u> ¹	0.1571	–
M_{HI}/M_{*}	0.1177	0.0622	4×10^{-7}
M_{H_2+HI}/M_{*}	0.7483 ¹	0.1571	–
$\log \text{SFR} [M_{\odot} \text{ yr}^{-1}]$	<u>0.0239</u>	0.2684	<u>0.0145</u>
$\log \text{sSFR} [\text{yr}^{-1}]$	<u>0.0495</u>	0.1843	0.012
$\log M_{H_2}/\text{SFR} [\text{yr}]$	0.0034 ¹	0.0036	–
$\log M_{HI}/\text{SFR} [\text{yr}]$	0.2406	0.4149	<u>0.0130</u>
$\log M_{H_2+HI}/\text{SFR} [\text{yr}]$	0.0855 ¹	0.3090	–

¹ Restricted mean and standard errors from the Kaplan-Meier estimator of the survival functions

Note: Underline indicate $p < 0.05$ and values are bolded for $p < 0.01$

Kolmogorov-Smirnov and log-rank statistical tests in order to determine whether the properties of the galaxies in these samples can be distinguished. We have decided to focus on the comparison between the group and Virgo samples, as they have roughly similar number of galaxies and CO detections, as compared to the field sample, which contains fewer galaxies. Future work will focus on further expanding the field sample and creating a sample of isolated galaxies, in order to incorporate these important objects into the analysis.

First, we consider the gas properties of the group and Virgo samples. The mean ratio of H₂ to HI gas mass is higher for the Virgo galaxies compared to the group galaxies. The log-rank test shows a significant difference in the distribution of the ratio of H₂ to HI between the Virgo sample and the field sample. This makes sense given that the Virgo galaxies have a lower mean HI gas masses and higher H₂ gas masses. This seems to follow the general trends from Kenney & Young (1989), who found that the Virgo galaxies are not as H₂ deficient as expected, given their HI deficiencies. The stellar mass normalized quantities, including the mean H₂ gas masses, generally follow the same trends as the unnormalized quantities. The difference between the stellar mass normalized HI mass distribution of the group and Virgo galaxies is not as significant as for the unnormalized case. The higher H₂ to HI ratio in the Virgo sample may indicate that these galaxies are more efficient at converting available HI to H₂, perhaps through the various forms of interactions that lead to gas flowing towards the centre of host galaxies and the creation of molecular hydrogen. An alternative explanation is that the cluster environment is more effective at stripping the HI rather than the H₂ gas and thus increasing the global H₂ to HI ratio (Pappalardo et al. 2012). These ideas will be explored in future studies with the resolved data.

With the H α data available for our galaxies, we can determine the star formation rates and specific star formation rates (star formation rate divided by stellar mass) for our galaxies. We find that both values are lower for Virgo galaxies, compared to the group galaxies. However, the Kolmogorov-Smirnov test shows that while the star formation rate distributions can be distinguished between the group and Virgo samples at higher significance than the specific star formation rates.

A method of measuring the relationship between star formation and the gas content of galaxies is through the gas depletion timescale ($M_{H_2}/\text{SFR} [\text{yr}]$) or its reciprocal, the star formation efficiency ($\text{SFR}/M_{H_2} [\text{yr}^{-1}]$). The mean log molecular gas depletion timescale is longer for the Virgo sample (8.97 ± 0.06) than for the group sample (8.44 ± 0.07), with the log-rank test showing that the Virgo galaxies can be distinguished from the group galaxies at the $p = 0.01$ level. This is shown graphically in Figure 2, where we see large differences in the shapes of the cumulative distribution functions. For the case where we only consider CO detected galaxies from the group and Virgo sample, the differences are still significant. When we calculate the gas depletion times with respect to the atomic hydrogen gas mass or the total gas mass (H₂ + HI), the two samples have similar distributions.

One possible explanation for this difference is metallicity effects on the X_{CO} value, as discussed in Section 2.2. If Virgo galaxies have systematically different metallicities than group galaxies, then that would have an effect on the molecular gas mass and hence the gas depletion times. The similar mean stellar mass of the two samples suggests any metallicity effects should not be significant. Other differences in the ISM properties, such as temperature or surface density, would also cause changes in the measured molecular gas mass, assuming a variable X_{CO} conversion factor prescription (Bolatto et al. 2013). However, it seems unlikely that Virgo spirals would have the extreme temperatures or surface densities required to cause a substantial difference in the X_{CO} factor.

Another explanation for the variations in the molecular gas depletion time is that star formation may be inhibited in the more extreme cluster environment, even in the presence of a comparable or even higher amount of H₂ gas, due to other mechanisms such as increasing thermal support in the gas. Turbulent pressure can play a large role in regulating star formation (Krumholz et al. 2009) and this pressure is likely to be different between the three environments. For example, studies of the dense gas tracer HCN in nearby disk galaxies from the HERACLES survey found variations in the star formation efficiency with environment and towards the centre of galaxies (Usero et al. 2015). The authors suggests models where such variations are caused by differences in the Mach number, which can also apply to the Virgo cluster environment. For example, Alatalo et al. (2015) found an increased ¹³CO/¹²CO ratio in early-type galaxies in the Virgo cluster, which they attribute to enrichment due to low-mass stars or to variations in the gas pressure in the dense environment. Another possibility is differences in the gravitational stability of spiral disks, which can be parametrized by the Toomre Q parameter (Toomre 1964; Kennicutt 1989). Close neighbors and the additional pressure from the cluster environment may cause changes in the disks of spiral galaxies and its star formation efficiency.

Comparing to previous surveys, we note that Leroy et al. (2008) found a constant value of the molecular gas depletion timescale of $(1.90 \pm 0.4) \times 10^9$ (or $\sim 10^{9.27}$) years using resolved maps of 23 galaxies from the HERACLES survey with CO $J = 2 - 1$ line, FUV + IR star formation rates, and a Kroupa IMF. The study of a sample of 30 galaxies from the HERACLES survey found a H₂ depletion timescale of 2.2×10^9 (or $\sim 10^{9.34}$) years (Leroy et al. 2013). This value is longer than our integrated values for our group and Virgo samples. The COLD GASS survey (Saintonge et al. 2011) found a molecular gas depletion time of ~ 1 Gyr, varying between ~ 0.5 Gyr for low-mass galaxies ($\sim 10^{10} M_{\odot}$) to ~ 3 Gyr for high-mass galaxies ($\sim 10^{11} M_{\odot}$). This is more similar to the results from the analysis of our sample of galaxies.

One reason for the variations in the molecular gas depletion

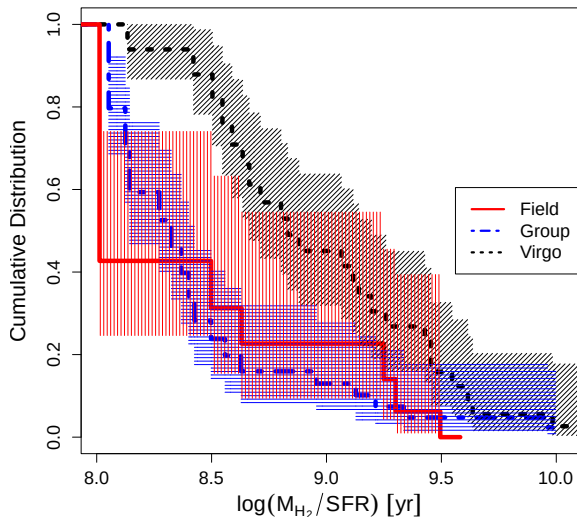


Figure 2. Survival functions for the molecular gas depletion time in the field (red solid line), group (blue dot-dash line), and Virgo (black dashed line) sample galaxies using the Kaplan-Meier estimator. The ‘steps’ in the distribution correspond to detections. The 95% confidence intervals are overlaid for the three distributions.

time between our sample and the HERACLES survey may be the difference between integrated and resolved measurements. We have calculated a single value of the molecular gas depletion time for the entire galaxy, as compared to performing pixel by pixel measurements. Leroy et al. (2013) found a median gas depletion time of 2.2 Gyr when weighted by individual measurements, but a lower value of 1.3 Gyr (or $\sim 10^{9.11}$ years) when weighted by galaxy. Second, the presence of lower mass galaxies in our sample could be driving down the mean molecular gas depletion timescale. This is because we are weighting all galaxies equally in this analysis, whereas resolved measurements are dominated by the measurements from larger, higher mass galaxies. Third, our use of the CO $J = 3 - 2$ line may be another reason, since that line traces a smaller fraction of the molecular gas than the CO $J = 2 - 1$ line, mainly the warmer and denser component. Although we have included an average line ratio in our calculations, we may still be missing some of the more diffuse gas in the disk. A fourth possibility is the difference in the star formation rate indicator ($H\alpha$ + extinction correction vs. FUV + IR), though it seems unlikely that the FUV + IR would provide systematically lower star formation rates. This is because the FUV component measures star formation on a longer timescale and both the FUV and IR have contributions not related to recent star formation (Kennicutt & Evans 2012). Finally, the $H\alpha$ emission may not fully coincide with the results from the CO maps, which for most observations were concentrated in the inner 2 arcminutes of the galaxy. This may lead to a higher star formation rate (measured over a larger portion of the galaxy) as compared to its gas content. A future extension to this project will look at resolved measurements for the galaxies in this sample, which will then create a more consistent comparison and may help resolve any differences.

3.3 CO Detected/Non-Detected Comparison

There are 44 CO detected galaxies in our sample, including 6 field galaxies, 17 group galaxies, and 21 Virgo galaxies. There are 54 CO non-detected galaxies, including 11 field galaxies, 25 group galaxies, and 18 Virgo galaxies. Looking at their gas properties, the two samples have roughly the same H I gas mass, which suggests the lack of a strong correlation between H_2 and H I gas masses in our H I - flux selected sample. The CO detected sample has a larger average stellar masses than the CO non-detected sample, as seen in the left panel of Figure 3. There is a very significant difference between their stellar mass distributions, with a corresponding p-value of 1×10^{-7} . The relationship between the stellar mass and CO detection would be expected if the H_2 gas mass is well-correlated with the stellar mass, which has also been seen in Boselli et al. (2014).

We also find that the upper limits for the H_2 and total gas mass in CO non-detected galaxies are lower than the corresponding values for the CO detected sample. However, the results are not as conclusive when considering the stellar mass normalized values. This is likely due to the large difference in the stellar mass of the two samples, with the CO detected galaxies being much more massive than the non-detected galaxies. This results in stellar-mass normalized H_2 and total gas masses that are comparable to the upper limits for CO detected sample. We will need more data to determine if there are any systematic differences between the two samples.

The mean log star formation rate is higher in the CO detected galaxies than in the CO non-detected galaxies (log SFR [$M_\odot \text{ yr}^{-1}$] of -0.35 ± 0.09 vs. -0.72 ± 0.07). The corresponding p-value for the Kolmogorov-Smirnov test between the two distributions is 0.0145. This difference in the star formation rates between the two samples is likely caused by the correlation between star formation rate and molecular gas, the material required to form stars. With the stellar masses of the CO detected galaxies substantially higher than those of the CO non-detected galaxies, the Kolmogorov-Smirnov test show a difference in the distribution of sSFR between the two samples, which can also be seen in the right panel of Figure 3. This is likely a consequence of the well-known negative correlation between stellar mass and specific star formation rate for star forming galaxies. Finally, the H I gas depletion times are longer in the CO non-detected galaxies compared to the CO non-detected galaxies. This is likely also due to the significant difference in their star formation rates.

3.4 CO $J = 3 - 2$ Detection Rates

The overall detection rate for the sample is 44 per cent. The CO $J = 3 - 2$ detection rate is slightly lower for the field (35 ± 9 per cent) sample, as compared to the group (40 ± 6 per cent) and Virgo (54 ± 9 per cent) samples. Some of the factors that would cause this difference include the Virgo galaxies being on average closer than the group and field galaxies, which can influence the CO detection rates, since closer galaxies would be easier to detect. Another important factor is sample variance and the smaller number of field galaxies in our sample, only 17 in total. As a result, the detection or non-detection of one or two galaxies can have a large influence on the CO detection rate.

We note that the stellar mass for the field sample is on average lower than the Virgo and group samples. Given the correlation between stellar mass and molecular gas mass (Lisenfeld et al. 2011; Boselli et al. 2014), this difference in the stellar mass will contribute to the difference in the detection rates. These low stellar mass galaxies (below $\sim 10^9 M_\odot$) may even be considered dwarf

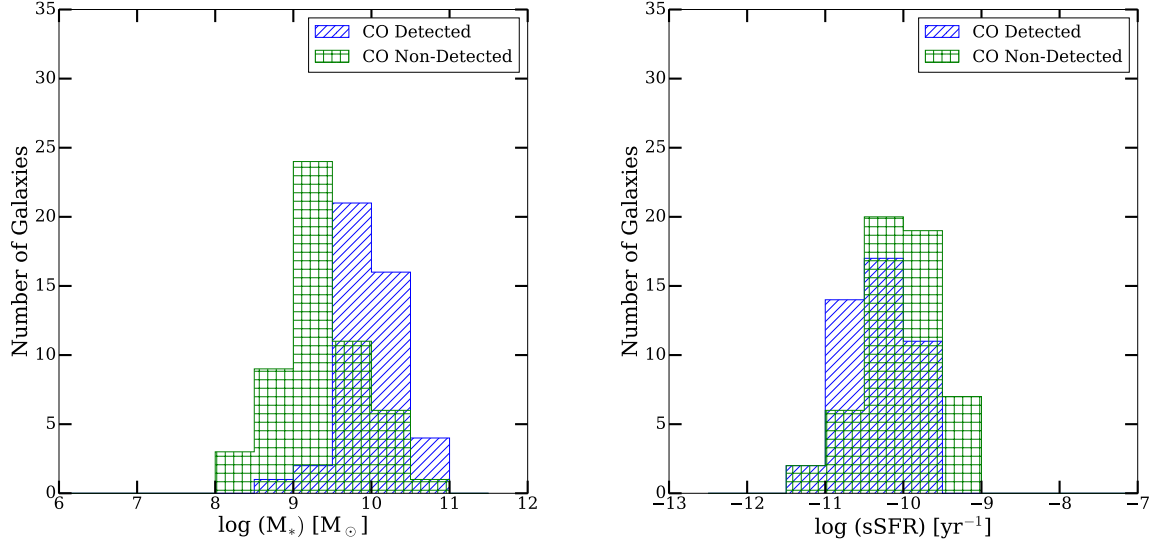


Figure 3. **Left:** A histogram showing the significant difference between the stellar mass distributions of the CO detected and non-detected samples ($p = 1 \times 10^{-9}$). **Right:** A histogram showing the difference in the sSFR distribution between the CO detected and non-detected samples ($p = 0.012$).

spirals according to the stellar mass classification from other galaxy surveys (Geha et al. 2012). In addition, if any galaxies in our sample are metal poor, this would also affect the H_2 mass we estimate via the metallicity dependence of the CO-to- H_2 conversion factor (Wilson 1995), as well as the detection rate. The stellar mass distribution of our field, group, and Virgo sample, with the majority of our galaxies in the mass range of $10^9 - 10^{11} M_\odot$, combined with the observed mass-metallicity relationship fit (Tremonti et al. 2004), would lead to $(12 + \log(O/H))$ values of between $8.63 - 9.11$. It is likely that few of these galaxies have metallicities more than a factor of two below solar ($12 + \log(O/H) = 8.69$), the rough limit at which any metallicity effects would become significant (Wilson 1995; Arimoto et al. 1996; Israel 2000; Bolatto et al. 2008).

Finally, the redshift-limited (recessional velocities of between 1500 and 5000 km s^{-1}) AMIGA survey of isolated galaxies detects $51 \pm 5\%$ in the CO $J = 1 - 0$ line, a detection rate similar to our Virgo samples and slightly higher than our overall sample (Lisenfeld et al. 2011). In comparison to our sample, their stellar masses (measured by L_K) are roughly in the range of $10^8 - 10^{11} M_\odot$, similar in mass to than our sample. Their sample of isolated galaxies is based on the catalogue of Karachentseva (1973) and is chosen to possess no nearby similarly sized neighbours in the sky.

4 DISCUSSION

4.1 Effects of Morphology

Morphology can have a large effect on the star formation (Kennicutt 1998a; Bendo et al. 2007) and the molecular gas properties (Kuno et al. 2007) of spiral galaxies. For our sample of galaxies, we have performed a simple comparison of the early-type spirals (a, ab, b, and bc) with the late-type spirals (c, cd, d, and m). As stated in the discussion of our sample selection in Section 2.1, we used the HyperLeda morphological codes for this classification, which employs a weighted average of multiple measurements. One galaxy classified as S?, NGC3077, is excluded from this analysis. In to-

Table 6. Significance Test Between Different Samples

Mean Quantity	Early/Late	Pair/Non-Pair
$\log M_{HI} [M_\odot]$	0.6553	0.9524
$\log M_{H_2} [M_\odot]^1$	0.0614	0.1799
$\log M_* [M_\odot]$	0.0013	0.4489
$\log M_{H_2+HI} [M_\odot]^1$	0.0504	0.8574
M_{H_2}/M_{HI}^1	0.0976	0.0098
M_{H_2}/M_*^1	0.3055	0.1971
M_{HI}/M_*	0.0014	<u>0.0450</u>
M_{H_2+HI}/M_*^1	<u>0.0066</u>	0.2072
$\log SFR [M_\odot \text{ yr}^{-1}]$	0.4178	0.4489
$\log sSFR [\text{yr}^{-1}]$	0.0620	0.5856
$\log M_{H_2}/SFR [\text{yr}]^1$	0.1249	<u>0.0163</u>
$\log M_{HI}/SFR [\text{yr}]$	0.2626	0.5856
$\log M_{H_2+HI}/SFR [\text{yr}]^1$	0.4890	0.8262

¹ Restricted mean and standard errors from the Kaplan-Meier estimator of the survival functions

Note: Underline indicate $p < 0.05$ and values are bolded for $p < 0.01$

tal, there are 40 early-type spirals and 57 late-type spirals. Selected properties for the two samples are presented in Table 5, as well as the results from the significance tests in Table 6.

The Kolmogorov-Smirnov test shows a significant difference in the stellar mass ($p = 0.0013$), with the mean value being higher for early-type spirals. This results in significantly lower stellar mass normalized HI gas masses and total gas masses for the sample. On the other hand, the Kolmogorov-Smirnov test shows that the distributions of HI mass, star formation rates, and the specific star formation rates are not significantly different between the two samples. Furthermore, the mean molecular gas mass and the molecular gas depletion times are not significantly different between the two samples. This suggests that variations between the early- and late-type spirals in this study should not be an important contributor to the differences observed between the group and Virgo samples.

Table 5. Selected Properties of the Early-type Spiral, Late-Type Spiral, Pair, and Non-Pair Populations

Mean Quantity	Early-type Spirals (40)	Late-type Spirals (57)	Pair (14)	Non-Pair (84)
$\log M_{HI} [M_{\odot}]$	9.13 ± 0.05	9.09 ± 0.04	9.06 ± 0.08	9.11 ± 0.03
$\log M_{H_2} [M_{\odot}]^1$	8.36 ± 0.08	8.00 ± 0.07	8.47 ± 0.13	8.06 ± 0.07
$\log M_* [M_{\odot}]$	9.86 ± 0.08	9.49 ± 0.07	9.79 ± 0.11	9.61 ± 0.06
$\log M_{H_2+HI}^1$	9.50 ± 0.07	9.25 ± 0.07	9.36 ± 0.08	9.35 ± 0.06
M_{H_2}/M_{HI}^1	0.63 ± 0.18	0.28 ± 0.10	1.09 ± 0.48	0.31 ± 0.07
M_{H_2}/M_*^1	0.055 ± 0.010	0.038 ± 0.007	0.066 ± 0.016	0.041 ± 0.006
M_{HI}/M_*	0.32 ± 0.06	0.70 ± 0.11	0.31 ± 0.07	0.59 ± 0.08
M_{H_2+HI}/M_*^1	0.40 ± 0.07	0.80 ± 0.13	0.38 ± 0.07	0.67 ± 0.09
$\log SFR [M_{\odot} \text{ yr}^{-1}]$	-0.44 ± 0.09	-0.62 ± 0.08	-0.46 ± 0.11	-0.57 ± 0.07
$\log sSFR [\text{yr}^{-1}]$	-10.30 ± 0.07	-10.10 ± 0.06	-10.26 ± 0.12	-10.18 ± 0.05
$\log M_{H_2}/SFR [\text{yr}]^1$	8.68 ± 0.10	8.55 ± 0.06	8.85 ± 0.20	8.57 ± 0.06
$\log M_{HI}/SFR [\text{yr}]$	9.57 ± 0.07	9.70 ± 0.05	9.52 ± 0.12	9.68 ± 0.05
$\log M_{H_2+HI}/SFR [\text{yr}]^1$	9.73 ± 0.06	9.79 ± 0.05	9.73 ± 0.11	9.78 ± 0.04

¹ Restricted mean and standard errors from the Kaplan-Meier estimator of the survival functions

4.2 Effects of Close Pairs

Interacting galaxies and mergers have been linked to more active star formation in their nucleus (Keel et al. 1985) and can lead to inflows of gas towards the centre (Mihos & Hernquist 1996), increased cooling, and greater fragmentation (Teyssier et al. 2010). From a large sample of SDSS galaxies, Ellison et al. (2008) found that there is a slight statistical enhancement in the star formation rate for close pairs. This enhancement is also seen for cases where these pairs actually undergo mergers and interactions (Knapen & James 2009; Knapen et al. 2015). However, this effect may be less apparent for galaxies that are inside denser environments (Ellison et al. 2010). Therefore, we decided to investigate the effects on our results of removing any close pairs from the sample. Once again, we use the catalog of Karachentsev (1972) to compare galaxies known to be in pairs with their non-pair counterparts. For the group sample, there are 5 galaxies in pairs (NGC0450, NGC2146A, NGC3507, NGC3455, NGC4123). For the Virgo sample, there are 9 galaxies in pairs (NGC4294, NGC4298, NGC4302, NGC4411A, NGC4430, NGC4561, NGC4567, NGC4568, NGC4647). Of these, 3 out of the 5 group galaxies and 5 out of 9 of the Virgo galaxies are CO detected. Note that for the galaxies in the Virgo cluster, close pairs may not be true interacting galaxies, due to the close proximity of these galaxies in the sky.

For most of the galaxy properties in this study, such as the stellar mass and atomic gas properties, the pair and non-pair samples are not significantly different. However, the H_2 to $H I$ gas mass ratio is higher and the H_2 gas depletion time is longer in the pair sample. From the significance tests in Table 6, the p-values are indicative of a significant difference between the two samples. These differences in the H_2 gas depletion time and the H_2 to $H I$ gas mass ratio are similar to those found when comparing between the group and Virgo galaxies. The various environmental effects, such as stripping of the atomic hydrogen in the outskirts and the interaction effects on the molecular gas, may also occur for the more extreme cases of close pairs.

We have also tested removing these pairs from our group and Virgo samples. Most of the results from our comparison of group and Virgo samples remain the same, such as the stellar masses and atomic gas properties. Virgo galaxies still possess a slightly higher mean molecular gas mass. On the other hand, while the H_2

to $H I$ ratio is higher for Virgo galaxies at 0.48 ± 0.14 compared to 0.25 ± 0.10 for the group galaxies, with the pairs removed the log-rank no longer shows a significant difference between the two distributions ($p = 0.1136$). Similarly, the mean $\log H_2$ gas depletion times [yr] for the Virgo galaxies is longer at 8.97 ± 0.06 compared to 8.44 ± 0.07 for the group sample, but now with a log-rank test value of $p = 0.079$.

These results suggest that these environmental trends in H_2 to $H I$ ratio and H_2 gas depletion times are similar when we make the comparison between the group/Virgo and between the pair/non-pair populations. Removing the presence of the Karachentsev (1972) pairs reduces the overall significance of the differences found between the group and Virgo samples. Physically, the environmental effects discussed in the previous section will likely be amplified for the galaxies that are strongly interacting. The question remains whether the observed variations in the molecular gas and star formation properties in the cluster environment affect all galaxies or whether the difference is mainly due to the denser environment producing more close pairs? A more systematic analysis is required to fully disentangle these two effects, such as increasing the number of galaxies in our sample, the use of a more rigorous method of defining pairs, and observing trends with distance to the cluster center or with multiple nearby clusters (such as the Fornax Cluster).

4.2.1 $H I$ Rich Galaxies

We have used the less traditional $H I$ flux as the primary selection in our sample of galaxies. As a result, our full sample includes many galaxies with normal $H I$ mass, but low stellar mass. We can see their presence most readily in the CO non-detected sample or by looking at the specific galaxies with high $H I$ gas mass to stellar mass ratios. In general, these objects will likely be missed by optically-selected surveys and may even exist as an understudied class of galaxies. Similar $H I$ rich objects have been observed recently by the Bluedisks project (Wang et al. 2013) and HighMass survey (Huang et al. 2014). The HighMass survey galaxies have high $H I$ gas mass ($M_{HI} > 10^{10} M_{\odot}$) and high $H I$ fractions compared to galaxies with the same stellar mass. After measuring their star formation rates, they found that the HighMass galaxies have comparatively high specific star formation rates, which the authors attribute to their more recent formation times. The CO non-detected

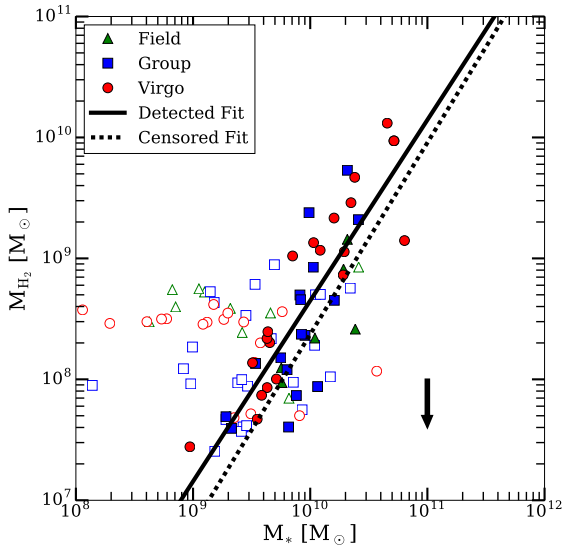


Figure 4. The molecular gas mass as a function of the stellar mass for the field, group, and Virgo sample. Filled points are detections while open points are upper limits, with the direction indicated by the large black arrow and a length of 1σ . Also plotted are the linear fit to the detected galaxies in the entire sample, with a slope of 1.49 ± 0.15 . The Pearson coefficient is 0.84 ($p = 7 \times 10^{-13}$). The Buckley-James fit produced a slope of 1.58 ± 0.15 . This relationship between the molecular gas mass and the stellar mass have been seen in previous survey for spiral galaxies (Lisenfeld et al. 2011; Boselli et al. 2014).

galaxies in our sample possess similar qualities, with lower stellar masses, high H I to stellar mass ratios, and higher specific star formation rates compared to the CO detected galaxies.

4.3 Correlation between Galaxy Properties

We seek to determine the important scaling relationships among the galaxies in our sample by plotting the different physical properties and identifying any possible correlations. For this analysis, we have chosen to use a simple linear fit to the CO detected galaxies, since the measurement errors on these galaxy properties are small compared to the scatter in the data points. To take into account the effects of data censoring for values along the y-axis, the Buckley-James estimator was used (Buckley & James 1979). To perform the Buckley-James regression, we used the subroutine BJ in the statistical package called RMS, which can be found at the standard R repository⁶. We have decided to use the Buckley-James regression in our analysis because of its similarity to survival analysis, with both techniques attempting to incorporate upper limits into the statistical treatment.

First, we present the relationship between stellar mass and molecular gas mass in Figure 4, which shows a positive correlation between the two parameters, with a slope of 1.49 ± 0.15 . This result indicates that the more massive galaxies in our sample contain more molecular gas and has been seen previously in Lisenfeld et al. (2011) for late-type galaxies. Boselli et al. (2014), using the Herschel Reference Survey, have also noted relatively constant

M_{H_2}/M_* ratios for spiral galaxies. On the whole, this result suggests that those galaxies with more stars have more fuel for future star formation.

Next, we show the relationship between the molecular gas mass and the star formation rate, which is similar to other analyses based on the Kennicutt-Schmidt law (Kennicutt 1998b). From the left panel in Figure 5, we find a considerable scatter around the fit. One difference from similar studies is the use of the CO $J = 3 - 2$ line, which traces denser and warmer molecular gas when compared to the lower transition CO lines. The use of CO and H α measurements covering different portions of the galaxies, as discussed when comparing integrated H $_2$ gas depletion times with other surveys, may also contribute to the scatter. Note that we have presented the plot as M_{H_2} vs star formation rate, since our method of calculating the censored data fit only allows for censoring for the variable in the y-axis. Previous studies of resolved molecular gas and star formation rate measurements have found a slope near unity (Bigiel et al. 2008; Leroy et al. 2013), though other groups have found larger values for the slope of the star formation rate vs. molecular gas mass (Kennicutt et al. 2007).

To determine the main cause of the large scatter, we have compared our results to an earlier paper in this series in the right panel of Figure 5. The previous paper focused on NGLS galaxies that are also found in the SINGS (Spitzer Infrared Nearby Galaxies Survey) sample. The star formation rates in Wilson et al. (2012) are measured using FIR fluxes instead of H α measurements, but they have been converted into star formation rates with the SF conversion factor from Kennicutt & Evans (2012), also assuming a Kroupa IMF. The galaxies from our larger sample seem to follow the same trend as the galaxies from Wilson et al. (2012), though with a much larger scatter. This scatter could be due to the marginal nature of some of our CO detections, as we have selected all galaxies with a S/N ratio > 3 . When we plot this relationship including only the galaxies in this paper with S/N > 5 , we find that the scatter is reduced, though not to the level from the Wilson et al. (2012) paper.

In addition, we can also look at the trends in the H $_2$ gas depletion time (molecular gas mass divided by the star formation rate) for the galaxies in our sample. In Figure 6, we find that there is a positive correlation between the molecular gas depletion time and the stellar mass, a result also noted in other surveys (Saintonge et al. 2011). The Pearson correlation parameter using the detected galaxies is 0.30 , which is weaker than the other correlations presented in this study. However, the p-value from the correlation is 0.047 , which is a strong hint that a correlation does exist. Saintonge et al. (2011) provide three possible explanations: bursty star formation in low mass galaxies reducing the star formation rates, a quenching mechanism that reduces the star formation efficiency in high mass galaxies, and/or observations not detecting a larger fraction of molecular gas in low mass galaxies. Other groups, such as Leroy et al. (2008), have not found any significant correlations between molecular gas depletion time and stellar mass. Furthermore, it has been suggested that this correlation would disappear with a mass-dependent CO conversion factor (Leroy et al. 2013).

Finally, in order to tie together three of the main parameters from our study (star formation, molecular gas mass, stellar mass), we explore the correlation between the specific star formation rate (sSFR) and the molecular gas depletion time. In Figure 7, we note a negative correlation between those two parameters, consistent with results from Saintonge et al. (2011), Huang & Kauffmann (2014), and Boselli et al. (2014). This correlation suggests that molecular gas is depleted more quickly in galaxies with high specific star formation rates (a high current star formation compared to their stel-

⁶ <http://cran.r-project.org/web/packages/rms/index.html>

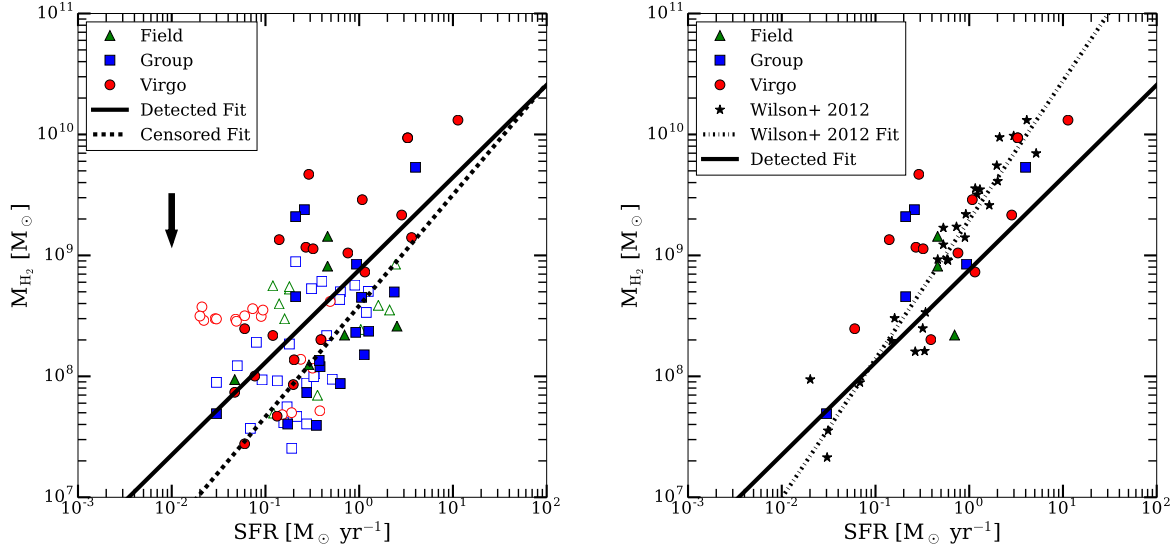


Figure 5. **Left:** The molecular gas mass as a function of the star formation rate for the field, group, and Virgo sample. Filled points are detections while open points are upper limits, with the direction indicated by the large black arrow and a length of 1σ . Also plotted are the linear fit to the detected galaxies in the entire sample, with a slope of 0.76 ± 0.14 . The corresponding Pearson coefficient is 0.64 ($p = 4 \times 10^{-6}$). The Buckley-James (censored) fit produced a slope of 0.92 ± 0.15 . **Right:** The molecular gas mass as a function of the star formation rate for the field, group, and Virgo sample, only including galaxies with a CO S/N ratio greater than 5. Also plotted in black stars are the smaller sample of galaxies from Wilson et al. (2012), which includes all NGLS galaxies that are also part of the Spitzer Infrared Nearby Galaxy Survey, with star formation rates are measured using FIR fluxes. The dotted line is the linear fit to the galaxies from Wilson et al. (2012) ($m = 1.149 \pm 0.005$), with the solid black line from the detected fit to the whole sample plotted for comparison purposes.

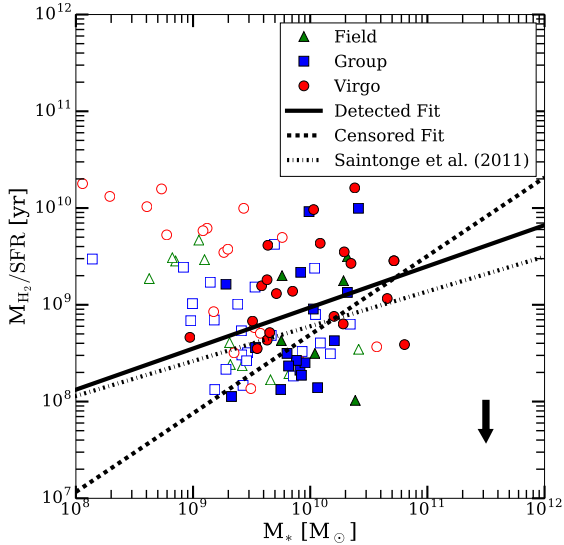


Figure 6. The molecular gas depletion time as a function of stellar mass for the field, group, and Virgo sample. Filled points are detections while open points are upper limits, with the direction indicated by the large black arrow and a length of 1σ . Also plotted are the linear fit to the detected galaxies in the entire sample, with a slope of 0.42 ± 0.21 and a Pearson coefficient of 0.30 ($p = 0.047$). The Buckley-James fit produced a steeper slope of 0.81 ± 0.22 . The results are compared to the fit from Saintonge et al. (2011) for a sample of 222 galaxies.

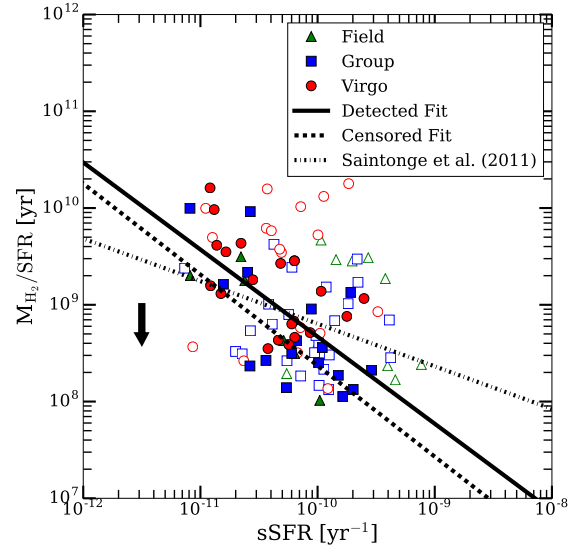


Figure 7. The molecular gas depletion time as a function of the specific star formation rate for the field, group, and Virgo sample. Filled points are detections while open points are upper limits, with the direction indicated by the large black arrow and a length of 1σ . Also plotted are the linear fit to the detected galaxies in the entire sample, with a slope of -0.90 ± 0.17 and a Pearson coefficient of -0.65 ($p = 2 \times 10^{-6}$). The Buckley-James fit produced a slope of -0.94 ± 0.16 . The results are compared to the fit from Saintonge et al. (2011) for a sample of 222 galaxies.

lar mass). In other words, the molecular gas depletion times inside galaxies are dependent on the fraction of new stars compared to the old stellar population. A related study by Kannappan et al. (2013) looked at the tight relationship between the fractional stellar mass growth rate (the mass of new stars formed over the past ~ 1 Gyr) and the gas to stellar mass ratio, which is suggestive of a link between the amount of new stars formed, the old stellar component, and the amount of gas available.

We note that the correlations found between the different galaxy properties in our sample were largely unchanged after subdividing between the group and Virgo sample, as seen in Figure 6 and Figure 7. The differences in slopes of the total sample and slopes of the group and Virgo sub-samples are within their respective error bars while the differences in the intercepts of these relations are likely related to the variations observed in the properties of the group and Virgo samples in the previous sections.

5 CONCLUSIONS

This paper presents the results of an analysis of an H I flux limited sample of 98 spiral galaxies from the Nearby Galaxies Legacy Survey (NGLS), a Virgo follow-up program, and selected galaxies from the Herschel Reference Survey (HRS). The sample was further subdivided into group and Virgo galaxies in order to determine any possible environmental effects. We studied their molecular gas content through CO $J = 3 - 2$ observations using the James Clerk Maxwell Telescope (JCMT) and star formation properties using H α measurements. We have also used survival analysis in order to incorporate data from galaxies with only upper limits on their CO measurements.

- The overall CO $J = 3 - 2$ detection rate for the galaxies in our sample is 44 per cent. The CO detected galaxies have a larger mean stellar mass and star formation rate compared to the CO non-detected galaxies. On the other hand, the mean specific star formation rates and H I gas masses are similar between the two samples.
- The mean log H I mass is larger for group galaxies compared to the Virgo galaxies, with the Kolmogorov-Smirnov test showing that the distribution of H I masses in the Virgo and group galaxies are significantly different. Conversely, the H₂ masses are higher in the Virgo compared to the group sample. As a result, the Virgo galaxies possess a significantly higher H₂ to H I ratio than the group sample. These galaxies inside the cluster may be better at converting their H I gas into H₂ gas, perhaps due to environmental effects on inflows towards the centre or the H₂ gas not being stripped as efficiently as the H I gas.
- The mean log molecular gas depletion time (M_{H_2}/SFR [yr]) is longer in the Virgo sample (8.97 ± 0.06) compared to the group (8.44 ± 0.07) sample. This difference in the molecular gas depletion time may be a combination of environmental factors that both increase the H₂ gas mass, as discussed in the previous point, and decrease the star formation rate in the presence of large amounts of molecular gas, such as heating processes in the cluster environment or differences in turbulent pressure (Usero et al. 2015; Alatalo et al. 2015).
- The molecular gas depletion time (M_{H_2}/SFR) depends positively on the stellar mass and negatively on the specific star formation rate, consistent with previous studies on these relationships (Saintonge et al. 2011; Boselli et al. 2014). Higher mass galaxies have a longer molecular gas depletion time, i.e., they are converting their molecular gas to stars at a slower rate. This may be caused by more bursty star formation in low mass galaxies and/or quenching

mechanisms in higher mass galaxies, as suggested by Saintonge et al. (2011). We find that galaxies with high specific star formation rates have shorter molecular gas depletion times, suggesting that galaxies with high star formation rates relative to their stellar populations would run out of fuel faster and may be undergoing a different and less sustainable star formation process. This is similar to results from other studies, including a large survey with nearby and high redshift galaxies, where Genzel et al. (2015) found that the gas depletion time depends most strongly on a galaxy's sSFR relative to the sSFR of the star-formation main sequence.

6 ACKNOWLEDGMENTS

We wish to thank the referee for their thorough review and useful suggestions. The James Clerk Maxwell Telescope has historically been operated by the Joint Astronomy Centre on behalf of the Science and Technology Facilities Council of the United Kingdom, the National Research Council of Canada and the Netherlands Organisation for Scientific Research. The research of C.D.W. is supported by grants from NSERC (Canada). We acknowledge financial support to the DAGAL network from the People Programme (Marie Curie Actions) of the European Unions Seventh Framework Programme FP7/2007-2013/ under REA grant agreement number PITN-GA-2011-289313, and from the Spanish Ministry of Economy and Competitiveness (MINECO) under grant number AYA2013-41243-P.

We acknowledge the usage of the HyperLeda database (<http://leda.univ-lyon1.fr>). This research has made use of the NASA/IPAC Extragalactic Database (NED) which is operated by the Jet Propulsion Laboratory, California Institute of Technology, under contract with the National Aeronautics and Space Administration. This publication makes use of data products from the Wide-field Infrared Survey Explorer, which is a joint project of the University of California, Los Angeles, and the Jet Propulsion Laboratory/California Institute of Technology, funded by the National Aeronautics and Space Administration. This work is based [in part] on archival data obtained with the Spitzer Space Telescope, which is operated by the Jet Propulsion Laboratory, California Institute of Technology under a contract with NASA. Support for this work was provided by an award issued by JPL/Caltech.

The Digitized Sky Surveys were produced at the Space Telescope Science Institute under U.S. Government grant NAG W-2166. The images of these surveys are based on photographic data obtained using the Oschin Schmidt Telescope on Palomar Mountain and the UK Schmidt Telescope. The plates were processed into the present compressed digital form with the permission of these institutions. The National Geographic Society - Palomar Observatory Sky Atlas (POSS-I) was made by the California Institute of Technology with grants from the National Geographic Society. The Second Palomar Observatory Sky Survey (POSS-II) was made by the California Institute of Technology with funds from the National Science Foundation, the National Geographic Society, the Sloan Foundation, the Samuel Oschin Foundation, and the Eastman Kodak Corporation. The Oschin Schmidt Telescope is operated by the California Institute of Technology and Palomar Observatory. The UK Schmidt Telescope was operated by the Royal Observatory Edinburgh, with funding from the UK Science and Engineering Research Council (later the UK Particle Physics and Astronomy Research Council), until 1988 June, and thereafter by the Anglo-Australian Observatory. The blue plates of the southern Sky Atlas and its Equatorial Extension (together known as the SERC-

J), as well as the Equatorial Red (ER), and the Second Epoch [red] Survey (SES) were all taken with the UK Schmidt.

REFERENCES

- Alatalo K. et al., 2015, *MNRAS*, 450, 3874
 Arimoto N., Sofue Y., Tsujimoto T., 1996, *PASJ*, 48, 275
 Baldry I. K., Balogh M. L., Bower R. G., Glazebrook K., Nichol R. C., Bamford S. P., Budavari T., 2006, *MNRAS*, 373, 469
 Bell E. F., McIntosh D. H., Katz N., Weinberg M. D., 2003, *ApJS*, 149, 289
 Bendo G. J. et al., 2007, *MNRAS*, 380, 1313
 Bigiel F., Leroy A., Walter F., Brinks E., de Blok W. J. G., Madore B., Thornley M. D., 2008, *AJ*, 136, 2846
 Bigiel F. et al., 2011, *ApJ*, 730, L13
 Binggeli B., Sandage A., Tammann G. A., 1985, *AJ*, 90, 1681
 Blanton M. R., Moustakas J., 2009, *ARA&A*, 47, 159
 Bolatto A. D., Leroy A. K., Rosolowsky E., Walter F., Blitz L., 2008, *ApJ*, 686, 948
 Bolatto A. D., Wolfire M., Leroy A. K., 2013, *ARA&A*, 51, 207
 Boselli A., Cortese L., Boquien M., Boissier S., Catinella B., Lagos C., Saintonge A., 2014, *A&A*, 564, A66
 Boselli A. et al., 2010, *PASP*, 122, 261
 Boselli A., Fossati M., Gavazzi G., Ciesla L., Buat V., Boissier S., Hughes T. M., 2015, *A&A*, 579, A102
 Buckle J. V. et al., 2009, *MNRAS*, 399, 1026
 Buckley J., James I., 1979, *Biometrika*, 66, 429
 Chamaraux P., Balkowski C., Gerard E., 1980, *A&A*, 83, 38
 Corbelli E. et al., 2012, *A&A*, 542, A32
 Elbaz D. et al., 2007, *A&A*, 468, 33
 Ellison S. L., Mendel J. T., Patton D. R., Scudder J. M., 2013, *MNRAS*, 435, 3627
 Ellison S. L., Patton D. R., Simard L., McConnachie A. W., 2008, *AJ*, 135, 1877
 Ellison S. L., Patton D. R., Simard L., McConnachie A. W., Baldry I. K., Mendel J. T., 2010, *MNRAS*, 407, 1514
 Eskew M., Zaritsky D., Meidt S., 2012, *AJ*, 143, 139
 Fumagalli M., Gavazzi G., 2008, *A&A*, 490, 571
 Garcia A. M., 1993, *A&AS*, 100, 47
 Gavazzi G., Boselli A., Donati A., Franzetti P., Scodreggio M., 2003, *A&A*, 400, 451
 Gavazzi G., Boselli A., van Driel W., O’Neil K., 2005, *A&A*, 429, 439
 Geha M., Blanton M. R., Yan R., Tinker J. L., 2012, *ApJ*, 757, 85
 Genzel R. et al., 2015, *ApJ*, 800, 20
 Gunn J. E., Gott III J. R., 1972, *ApJ*, 176, 1
 Hafok H., Stutzki J., 2003, *A&A*, 398, 959
 Haynes M. P., Giovanelli R., 1986, *ApJ*, 306, 466
 Huang M.-L., Kauffmann G., 2014, *MNRAS*, 443, 1329
 Huang S. et al., 2014, *ApJ*, 793, 40
 Iono D. et al., 2009, *ApJ*, 695, 1537
 Israel F., 2000, in Combes F., Pineau Des Forets G., eds, *Molecular Hydrogen in Space*. p. 293
 Israel F. P., 1997, *A&A*, 328, 471
 Kannappan S. J. et al., 2013, *ApJ*, 777, 42
 Kaplan E. L., Meier P., 1958, *J. Amer. Statist. Assn.*, 53, 457
 Karachentsev I. D., 1972, *Soobshcheniya Spetsial’noj Astrofizicheskoy Observatorii*, 7, 1
 Karachentseva V. E., 1973, *Soobshcheniya Spetsial’noj Astrofizicheskoy Observatorii*, 8, 3
 Keel W. C., Kennicutt Jr. R. C., Hummel E., van der Hulst J. M., 1985, *AJ*, 90, 708
 Kenney J. D. P., Young J. S., 1989, *ApJ*, 344, 171
 Kennicutt R. C., Evans N. J., 2012, *ARA&A*, 50, 531
 Kennicutt Jr. R. C., 1989, *ApJ*, 344, 685
 Kennicutt Jr. R. C., 1998a, *ARA&A*, 36, 189
 Kennicutt Jr. R. C., 1998b, *ApJ*, 498, 541
 Kennicutt Jr. R. C. et al., 2007, *ApJ*, 671, 333
 Kennicutt Jr. R. C. et al., 2009, *ApJ*, 703, 1672
 Knapen J. H., Cisternas M., Querejeta M., 2015, *MNRAS*, 454, 1742
 Knapen J. H., James P. A., 2009, *ApJ*, 698, 1437
 Knapp G. R., Helou G., Stark A. A., 1987, *AJ*, 94, 54
 Koopmann R. A., Haynes M. P., Catinella B., 2006, *AJ*, 131, 716
 Kroupa P., Weidner C., 2003, *ApJ*, 598, 1076
 Krumholz M. R., McKee C. F., Tumlinson J., 2009, *ApJ*, 699, 850
 Kuno N. et al., 2007, *PASJ*, 59, 117
 Larson R. B., Tinsley B. M., Caldwell C. N., 1980, *ApJ*, 237, 692
 Leroy A. K. et al., 2012, *AJ*, 144, 3
 Leroy A. K., Walter F., Brinks E., Bigiel F., de Blok W. J. G., Madore B., Thornley M. D., 2008, *AJ*, 136, 2782
 Leroy A. K. et al., 2013, *AJ*, 146, 19
 Lisenfeld U. et al., 2011, *A&A*, 534, A102
 Makarov D., Prugniel P., Terekhova N., Courtois H., Vauglin I., 2014, *A&A*, 570, A13
 Mantel N., 1966, *Cancer Chemother Rep.*, 50, 163
 Mei S. et al., 2007, *ApJ*, 655, 144
 Mihos J. C., Hernquist L., 1996, *ApJ*, 464, 641
 Moore B., Katz N., Lake G., Dressler A., Oemler A., 1996, *Nature*, 379, 613
 Pappalardo C. et al., 2012, *A&A*, 545, A75
 Paturel G., Petit C., Prugniel P., Theureau G., Rousseau J., Brouty M., Dubois P., Cambrésy L., 2003, *A&A*, 412, 45
 Portinari L., Sommer-Larsen J., Tantalo R., 2004, *MNRAS*, 347, 691
 Saintonge A. et al., 2011, *MNRAS*, 415, 61
 Sánchez-Gallego J. R., Knapen J. H., Wilson C. D., Barmby P., Azimlu M., Courteau S., 2012, *MNRAS*, 422, 3208
 Sheth K. et al., 2010, *PASP*, 122, 1397
 Skrutskie M. F. et al., 2006, *AJ*, 131, 1163
 Solanes J. M., Manrique A., García-Gómez C., González-Casado G., Giovanelli R., Haynes M. P., 2001, *ApJ*, 548, 97
 Stark A. A., Knapp G. R., Bally J., Wilson R. W., Penzias A. A., Rowe H. E., 1986, *ApJ*, 310, 660
 Strateva I. et al., 2001, *AJ*, 122, 1861
 Strong A. W. et al., 1988, *A&A*, 207, 1
 Teyssier R., Chapon D., Bournaud F., 2010, *ApJ*, 720, L149
 Toomre A., 1964, *ApJ*, 139, 1217
 Tremonti C. A. et al., 2004, *ApJ*, 613, 898
 Usero A. et al., 2015, *AJ*, 150, 115
 Vollmer B., Wong O. I., Braine J., Chung A., Kenney J. D. P., 2012, *A&A*, 543, A33
 Wang J. et al., 2013, *MNRAS*, 433, 270
 Wilson C. D., 1995, *ApJ*, 448, L97
 Wilson C. D. et al., 2012, *MNRAS*, 424, 3050
 Wilson C. D. et al., 2009, *ApJ*, 693, 1736
 Young L. M. et al., 2011, *MNRAS*, 414, 940

APPENDIX A: COMPARISON OF THE THREE CO DATASETS

We present plots of selected properties from the three observing programs that make up our sample in Figure A1. There is a large difference in the distribution of distances between the three datasets, as the NGLS and Virgo follow-up have an obvious peak at our assumed Virgo distance of 16.7 Mpc. For the atomic hydrogen mass, there is only a significant difference between the distributions of the Virgo follow-up and the HRS ($p = 0.003$) datasets using the Kolmogorov-Smirnov test, likely due to the Virgo follow-up program only containing Virgo galaxies. For the sSFR, we only find a small difference between the distributions for the NGLS and the HRS datasets ($p = 0.036$). For the stellar mass distributions, we find no significant differences using the Kolmogorov-Smirnov test. Finally, for the molecular gas mass, we use the log-rank test to find the only significant difference is between the NGLS and the HRS datasets ($p = 0.003$), where the resulting mean molecular gas mass is lower in the HRS dataset.

Any differences between the samples can be attributed to the small numbers of galaxies in each dataset and to the percentage of galaxies in each environment, since our sample criteria is very similar between the three datasets. For example, the original NGLS dataset contain roughly equal numbers of group and Virgo galaxies, with a smaller number of field galaxies. The Virgo follow-up only contains Virgo galaxies. The HRS, which contains galaxies not already in the sample from the NGLS and Virgo follow-up, is skewed towards group galaxies. Given that the three datasets trace the environment differently, that is likely one of the main causes of the observed variations.

APPENDIX B: SELECTED PROPERTIES OF THE GALAXIES IN OUR SAMPLE

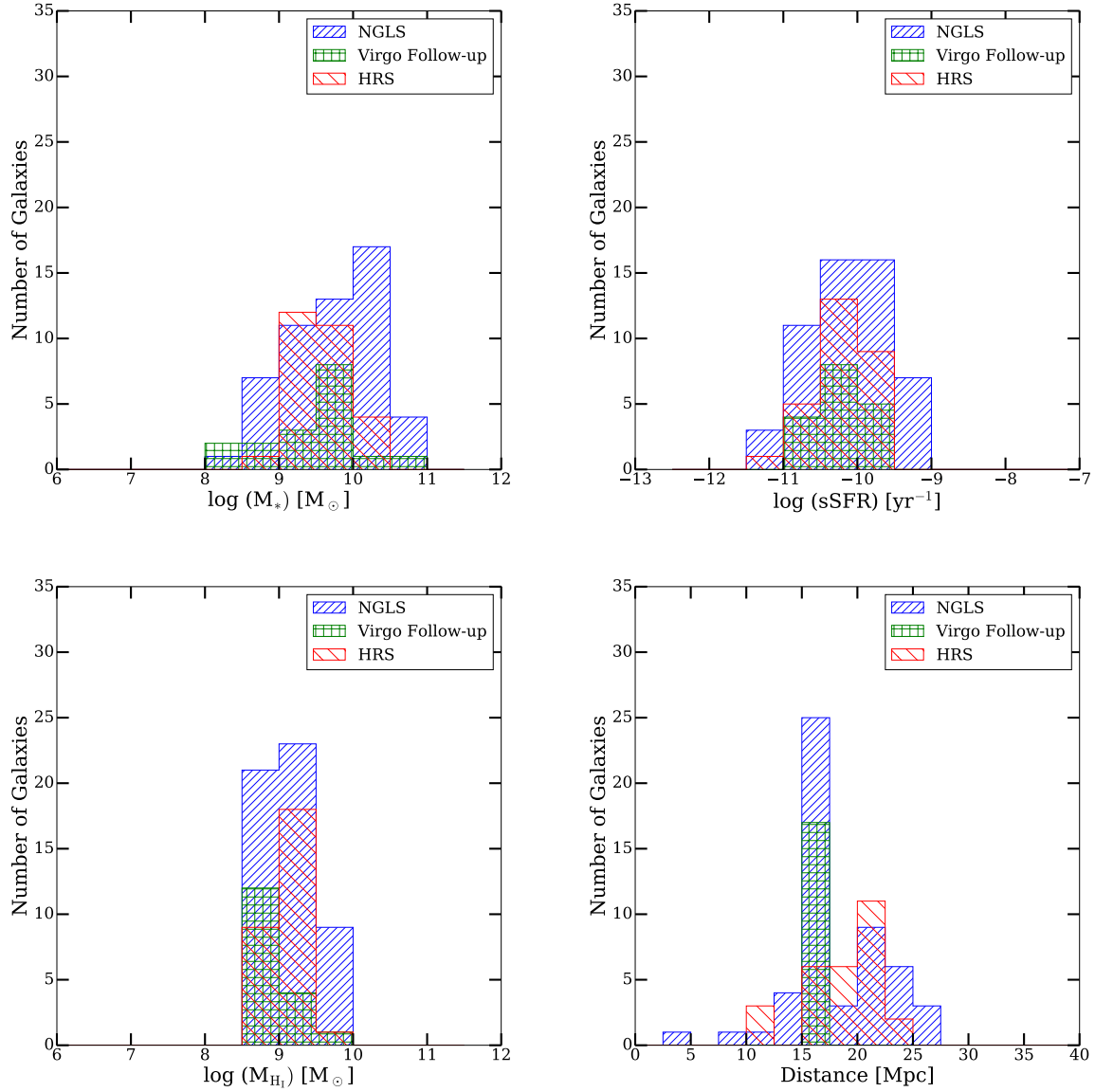


Figure A1. We present histograms of selected properties of the three sample sources, the NGLS, Virgo follow-up sample, and the additional HRS galaxies. The properties presented are stellar mass (top left), sSFR (top right), H I mass (bottom left), and distance (bottom right).

Table B1. Selected Properties of Field Galaxies

Name	Type ¹	D_{25} ¹ (kpc)	Distance ² (Mpc)	ΔT ³ (mK)	$L_{CO(3-2)}$ ⁴ (10^7 K km s ⁻¹ pc ²)	$\log(M_{HI})$ ⁵ (M_{\odot})	$\log(M_{H_2})$ ⁶ (M_{\odot})	$\log(M_*)$ ⁷ (M_{\odot})	SFR ⁸ (M_{\odot} yr ⁻¹)
ESO477-016	Sbc	16.5	24.2	16	< 1.48	9.06	< 8.72	9.10	0.18
ESO570-019	Sc	7.4	18.4	21	< 1.12	9.13	< 8.60	8.85	0.14
IC1254	SABb	5.8	21.9	21	< 1.57	8.90	< 8.75	9.05 [†]	0.12
NGC0210	SABb	32.7	22.4	25	1.46 ± 0.47	9.79	8.42	10.38 [†]	2.53
NGC6118	Sc	31.4	24.2	26	< 2.38	9.54	< 8.93	10.41	2.44
NGC6140	Sc	10.8	17.8	20	< 0.99	9.67	< 8.55	9.66	2.11
NGC7742	Sb	12.3	24.8	20	4.58 ± 0.84	9.09	8.91	10.28	0.46
PGC045195	Sd	21.9	20.7	16	< 1.09	9.48	< 8.59	9.32	1.60
PGC057723	SABb	7.9	14.9	20	< 0.69	9.31	< 8.39	9.42 [†]	1.04
UGC06378	Sc	13.0	23.0	19	< 1.55	9.12	< 8.74	8.82	0.18
UGC06792	Sc	10.1	15.5	23	< 0.84	8.79	< 8.48	8.63	0.16
NGC4013	Sb	22.1	15.5	19	8.08 ± 1.04	9.15	9.16	10.32	0.46
NGC3437**	SABc	13.7	20.1	23	1.23 ± 0.23	9.11	8.34	10.04	0.70
NGC3485**	Sb	13.9	21.9	22	< 0.20	9.46	< 7.84	9.82	0.36
NGC3501**	Sc	22.1	17.8	25	0.53 ± 0.15	8.99	7.97	9.76	0.05
NGC3526**	Sc	14.9	21.3	16	< 0.14	8.95	< 7.70	9.31	0.12
NGC3666**	SBC	16.8	16.7	17	0.70 ± 0.16	9.36	8.09	9.75	0.29

Note: ** next to name indicates that the galaxy is from the HRS program

¹ Morphologies and D_{25} extracted from HyperLeda database

² Distances extracted from HyperLeda, corrected for Virgo infall and assuming $H_0 = 70$ km s⁻¹ Mpc⁻¹, $\Omega_M = 0.27$, $\Omega_{\Lambda} = 0.73$

³ RMS noise in individual spectra in the data cube at 20 km s⁻¹ resolution on T_{MB} scale

⁴ Upper limits are 2σ limits calculated over an area of 1' and a line width of 100 km s⁻¹

⁵ M_{HI} calculated using values for H1 flux from HyperLeda database

⁶ M_{H_2} calculated assuming a CO $J = 3 - 2/J = 1 - 0$ line ratio of 0.18

⁷ $\log(M_*)$ from the S⁴G survey (Sheth et al. 2010), except for galaxies with [†] symbol, where $\log(M_*)$ is from K-band luminosity assuming stellar mass-to-light ratio of 0.533 (Portinari et al. 2004)

⁸ Star formation rates from Sánchez-Gallego et al. (2012) for NGLS galaxies, Boselli et al. (2015) for HRS galaxies

Table B2. Selected Properties of Group Galaxies

Name	Type ¹	D_{25} ¹ (kpc)	Distance ² (Mpc)	ΔT ³ (mK)	$L_{CO(3-2)}$ ⁴ ($10^7 \text{ K km s}^{-1} \text{ pc}^2$)	$\log(M_{HI})$ ⁵ (M_{\odot})	$\log(M_{H_2})$ ⁶ (M_{\odot})	$\log(M_*)$ ⁷ (M_{\odot})	SFR ⁸ ($M_{\odot} \text{ yr}^{-1}$)	Group ID ⁹
IC0750	Sab	8.3	13.7	25	13.41 ± 0.97	8.92	9.38	9.99	0.26	269
IC1066	Sb	8.5	24.2	19	< 1.71	9.02	< 8.79	9.53	0.40	387
NGC0450	SABc	21.8	25.4	20	0.85 ± 0.22	9.46	8.18	9.75	1.13	P
NGC0615	Sb	23.8	25.9	15	< 1.60	9.42	< 8.75	10.34	0.90	27
NGC1140	SBm	11.9	20.1	15	< 0.95	9.39	< 8.53	9.45	1.19	71
NGC1325	SBbc	26.3	20.7	21	< 1.40	9.29	< 8.70	10.05	0.63	97
NGC2146A	SABc	20.3	25.9	24	< 2.49	9.56	< 8.95	9.69 [†]	0.21	P
NGC2742	Sc	18.8	22.4	24	2.53 ± 0.83	9.27	8.65	10.21	1.06	167
NGC3077	S?	6.0	3.9	26	0.28 ± 0.05	9.12	7.69	9.28	0.03	176
NGC3162	SABc	12.6	20.7	22	2.80 ± 0.66	9.41	8.70	9.91	2.36	194
NGC3227	SABa	21.3	18.4	25	11.74 ± 1.29	8.99	9.32	10.41	0.21	194
NGC3254	Sbc	14.9	21.9	19	< 1.42	9.56	< 8.70	10.09	1.25	197
NGC3353	Sb	6.7	17.2	26	< 1.21	8.88	< 8.64	9.18	0.62	201
NGC3507	SBb	13.3	15.5	21	1.30 ± 0.42	8.95	8.36	9.96	0.92	228
NGC3782	Scd	5.1	14.3	21	< 0.52	9.01	< 8.27	9.00	0.18	258
NGC4041	Sbc	16.4	21.9	22	30.09 ± 2.52	9.56	9.73	10.32	3.99	266
NGC4288	SBcd	5.7	11.5	21	< 0.34	8.92	< 8.09	8.92	0.05	269
NGC4504	SABc	13.7	14.9	18	< 0.61	9.51	< 8.34	9.67	0.45	293
NGC4772	Sa	19.1	16.1	17	< 0.54	8.82	< 8.28	10.04	0.08	292
NGC5477	Sm	2.7	8.6	22	< 0.25	8.80	< 7.95	8.14	0.03	371
NGC5486	Sm	9.5	24.2	16	< 1.49	9.18	< 8.72	9.15	0.31	373
IC3908**	SBcd	13.6	19.0	13	2.56 ± 0.25	8.96	8.66	9.92	0.21	314
NGC3346**	SBc	14.9	19.5	19	0.41 ± 0.13	9.09	7.87	9.88	0.28	214
NGC3370**	Sc	14.4	20.1	26	< 0.27	9.26	< 7.98	9.86	0.52	219
UGC06023**	SBcd	10.3	21.3	24	< 0.25	8.98	< 7.94	9.46	0.28	227
NGC3455**	SABb	11.5	17.2	22	< 0.13	8.96	< 7.67	9.28	0.22	219
NGC3681**	Sbc	9.9	19.5	20	< 0.16	9.37	< 7.75	9.93	0.17	237
NGC3684**	Sbc	12.3	18.4	22	0.68 ± 0.20	9.37	8.08	9.80	0.38	237
NGC3756**	SABb	12.4	22.4	26	< 0.29	9.36	< 8.02	10.17	0.34	250
NGC3795**	Sbc	12.9	21.3	26	< 0.26	8.89	< 7.97	9.38	0.09	244
NGC3982**	SABb	12.5	20.1	26	4.76 ± 0.81	9.22	8.93	10.03	0.94	250
NGC4123**	Sc	18.5	20.1	28	0.49 ± 0.16	9.56	7.94	10.06	0.63	275
NGC4668**	SBcd	11.2	24.2	24	< 0.28	9.11	< 8.00	9.42	0.33	299
NGC4688**	Sc	16.8	15.5	29	< 0.11	9.15	< 7.61	9.43	0.28	292
NGC4701**	Sc	5.8	11.5	26	< 0.07	9.02	< 7.41	9.19	0.19	292
NGC4713**	Scd	5.3	10.9	12	0.22 ± 0.06	9.03	7.60	9.33	0.35	315
NGC4771**	Sc	15.5	17.2	13	0.23 ± 0.07	8.94	7.61	9.82	0.17	315
NGC4775**	Scd	15.0	23.0	12	1.33 ± 0.42	9.46	8.37	9.92	1.26	314
NGC4808**	Sc	8.2	12.0	25	0.76 ± 0.17	9.28	8.13	9.53	0.37	315
UGC06575**	Sc	11.0	21.3	27	< 0.26	9.15	< 7.96	8.98	0.13	244
UGC07982**	Sc	14.9	17.8	13	< 0.10	8.69	< 7.57	9.41	0.07	315
UGC08041**	SBcd	18.5	20.1	12	< 0.12	9.19	< 7.62	9.46	0.16	315

Note: ** next to name indicates that the galaxy is from the HRS program

¹ Morphologies and D_{25} extracted from HyperLeda database

² Distances extracted from HyperLeda, corrected for Virgo infall and assuming $H_0 = 70 \text{ km s}^{-1} \text{ Mpc}^{-1}$, $\Omega_M = 0.27$, $\Omega_{\Lambda} = 0.73$

³ RMS noise in individual spectra in the data cube at 20 km s^{-1} resolution on T_{MB} scale

⁴ Upper limits are 2σ limits calculated over an area of $1'$ and a line width of 100 km s^{-1}

⁵ M_{HI} calculated using values for H I flux from HyperLeda database

⁶ M_{H_2} calculated assuming a CO $J = 3 - 2/J = 1 - 0$ line ratio of 0.18

⁷ $\log(M_*)$ from the S⁴G survey (Sheth et al. 2010), except for galaxies with [†] symbol, where $\log(M_*)$ is from K-band luminosity assuming stellar mass-to-light ratio of 0.533 (Portinari et al. 2004)

⁸ Star formation rates from Sánchez-Gallego et al. (2012) for NGLS galaxies, Boselli et al. (2015) for HRS galaxies

⁹ Group IDs from Garcia (1993), while P indicates pairs from Karachentsev (1972)

Table B3. Selected Properties of Virgo Galaxies

Name	Type ¹	D_{25} ¹ (kpc)	Distance ² (Mpc)	ΔT ³ (mK)	$L_{CO(3-2)}$ ⁴ (10^7 K km s ⁻¹ pc ²)	$\log(M_{HI})$ ⁵ (M_{\odot})	$\log(M_{H_2})$ ⁶ (M_{\odot})	$\log(M_*)$ ⁷ (M_{\odot})	SFR ⁸ (M_{\odot} yr ⁻¹)
IC3061*	SBc	22.9	16.7	22	< 0.83	8.70	< 8.47	9.12	0.05
IC3074*	SBd	2.9	16.7	19	< 0.84	8.89	< 8.48	8.61 [†]	0.03
IC3322A*	SBc	8.8	16.7	21	0.26 ± 0.07	9.09	7.67	9.55	0.13
IC3371*	Sc	5.1	16.7	21	< 0.81	8.68	< 8.46	8.29	0.02
IC3576*	SBm	11.1	16.7	21	< 0.89	8.95	< 8.50	8.77	0.06
NGC4206	Sbc	16.3	16.7	14	0.48 ± 0.14	9.38	7.93	9.63	0.20
NGC4254	Sc	52.9	16.7	27	73.80 ± 2.51	9.66	10.12	10.66	11.31
NGC4273*	Sc	22.4	16.7	23	5.88 ± 0.69	8.95	9.02	9.85	0.76
NGC4298	Sc	13.4	16.7	21	6.56 ± 1.16	8.84	9.07	10.08	0.27
NGC4303A	Sbc	47.5	16.7	26	52.64 ± 5.72	9.65	9.97	10.71	3.29
NGC4302*	Sc	32.3	16.7	14	6.37 ± 0.91	9.28	9.05	10.29	0.32
NGC4303*	Sbc	47.5	16.7	26	52.64 ± 5.72	9.65	9.97	10.71	3.29
NGC4316*	Sc	13.9	16.7	22	0.56 ± 0.16	8.70	8.00	9.71	0.08
NGC4330*	Sc	16.9	16.7	24	0.41 ± 0.14	8.68	7.87	9.59	0.05
NGC4383	Sa	12.8	16.7	20	1.13 ± 0.22	9.16	8.30	9.65	0.39
NGC4390	SABc	7.6	16.7	19	< 0.88	8.63	< 8.50	9.26	0.09
NGC4411A*	Sc	9.5	16.7	23	< 0.80	8.65	< 8.46	9.08	0.05
NGC4411B*	SABc	10.8	16.7	22	< 0.99	8.91	< 8.55	9.30	0.09
NGC4423	Sd	10.2	16.7	18	0.16 ± 0.05	8.91	7.44	8.97	0.06
NGC4430	Sb	13.3	16.7	17	1.22 ± 0.40	8.62	8.34	9.63	0.12
NGC4470	Sa	13.2	16.7	19	< 0.84	8.68	< 8.47	9.43	0.03
NGC4480*	SABc	20.1	16.7	20	0.77 ± 0.24	8.87	8.14	9.51	0.20
NGC4498*	Sc	19.8	16.7	24	< 0.78	8.77	< 8.14	9.52	0.24
NGC4519*	Scd	13.0	16.7	22	< 1.12	9.49	< 8.30	9.57	0.39
NGC4522	SBc	35.5	16.7	13	1.39 ± 0.21	8.72	8.39	9.64	0.06
NGC4548	Sb	14.7	16.7	35	< 0.33	8.86	< 8.07	10.57	0.32
NGC4561	SBcd	8.6	16.7	26	< 1.17	9.11	< 8.62	9.18	0.49
NGC4567	Sbc	27.2	16.7	20	7.58 ± 0.99	9.02	9.13	10.03	0.14
NGC4568	Sbc	42.2	16.7	19	26.30 ± 1.98	8.88	9.67	10.38	0.29
NGC4579	SABb	34.4	16.7	20	7.89 ± 2.51	8.79	9.15	10.80	3.62
NGC4639	Sbc	13.5	16.7	20	< 0.28	8.97	< 7.70	9.91	0.19
NGC4647	SABc	17.5	16.7	23	12.11 ± 1.86	8.70	9.33	10.20 [†]	2.84
NGC4651	Sc	15.5	16.7	19	4.10 ± 0.79	9.47	8.86	10.28	1.15
NGC4654	Sc	22.7	16.7	12	16.22 ± 1.61	9.49	9.46	10.35	1.08
PGC040604*	SBm	5.3	16.7	24	< 1.05	8.64	< 8.57	8.06 [†]	0.02
UGC07557*	SABm	11.9	16.7	24	< 1.02	9.03	< 8.56	9.76	0.07
UGC07590	Sbc	6.1	16.7	19	< 0.89	8.87	< 8.50	8.73	0.02
NGC4294**	SBc	11.7	16.7	24	< 0.15	9.20	< 7.71	9.49	0.38
NGC4396**	Scd	13.6	16.7	25	< 0.14	8.87	< 7.68	9.35 [†]	0.15

Note: * indicates galaxy is in the Virgo follow-up program, ** indicates that the galaxy is from the HRS program

¹ Morphologies and D_{25} extracted from HyperLeda database

² Distances set to be at 16.7 Mpc (Mei et al. 2007)

³ RMS noise in individual spectra in the data cube at 20 km s⁻¹ resolution on T_{MB} scale

⁴ Upper limits are 2σ limits calculated over an area of 1' and a line width of 100 km s⁻¹

⁵ M_{HI} calculated using values for HI flux from HyperLeda database

⁶ M_{H_2} calculated assuming a CO $J = 3 - 2/J = 1 - 0$ line ratio of 0.18

⁷ $\log(M_*)$ from the S⁴G survey (Sheth et al. 2010), except for galaxies with [†] symbol, where $\log(M_*)$ is from K-band luminosity assuming stellar mass-to-light ratio of 0.533 (Portinari et al. 2004)

⁸ Star formation rates from Sánchez-Gallego et al. (2012) for NGLS galaxies, GOLDMine database for the Virgo follow-up (Gavazzi et al. 2003), and Boselli et al. (2015) for HRS galaxies

APPENDIX C: CO $J = 3 - 2$ MAPS OF NGLS GALAXIES

We present the CO $J = 3 - 2$ maps of our sample of galaxies from the Nearby Galaxies Legacy Survey.

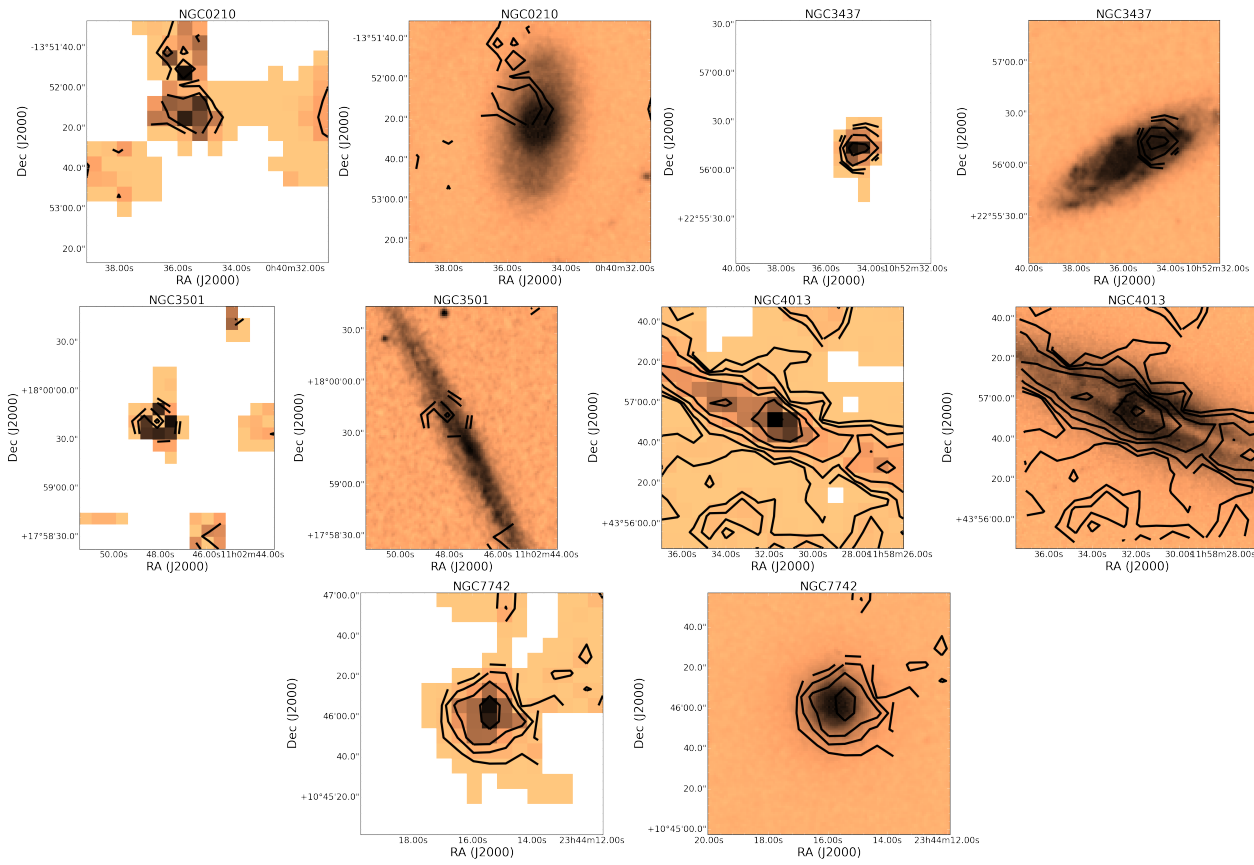


Figure C1. Images of the CO detected galaxies in the field sample. There are two plots for each galaxy. The first panel in each pair is the CO $J = 3 - 2$ integrated galaxy map with black contour levels overlaid at 0.5, 1, and 2 K km s^{-1} . The second panel is the same contour levels overlaid on the optical image from the Digitized Sky Survey.

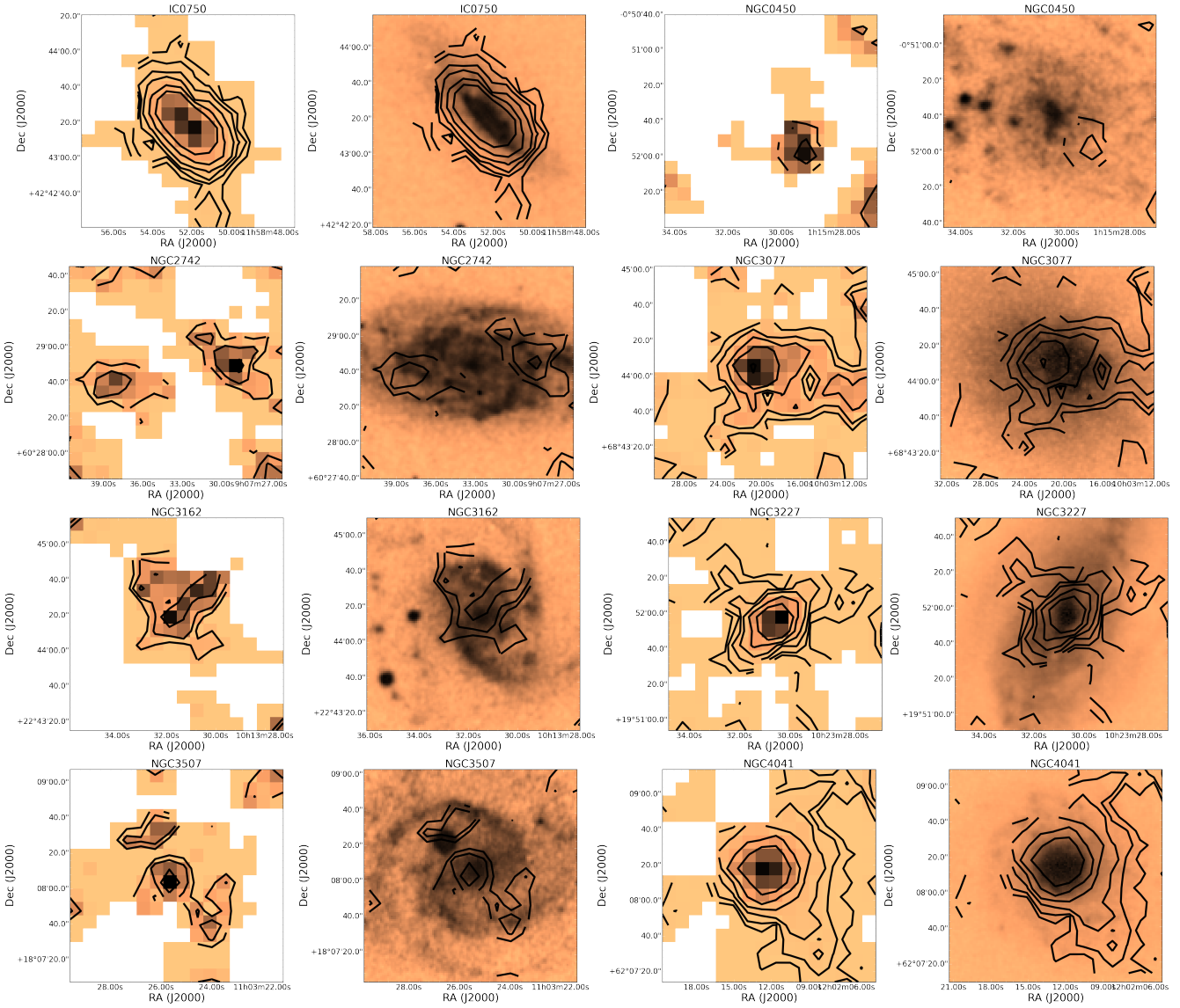


Figure C2. Images of the CO detected galaxies in the group sample. The first panel in each pair is the CO $J = 3 - 2$ integrated galaxy map with black contour levels overlaid at 0.5, 1, 2, 4, 8, and 16 K m s^{-1} . The second panel is the same contour levels overlaid on the optical image from the Digitized Sky Survey.

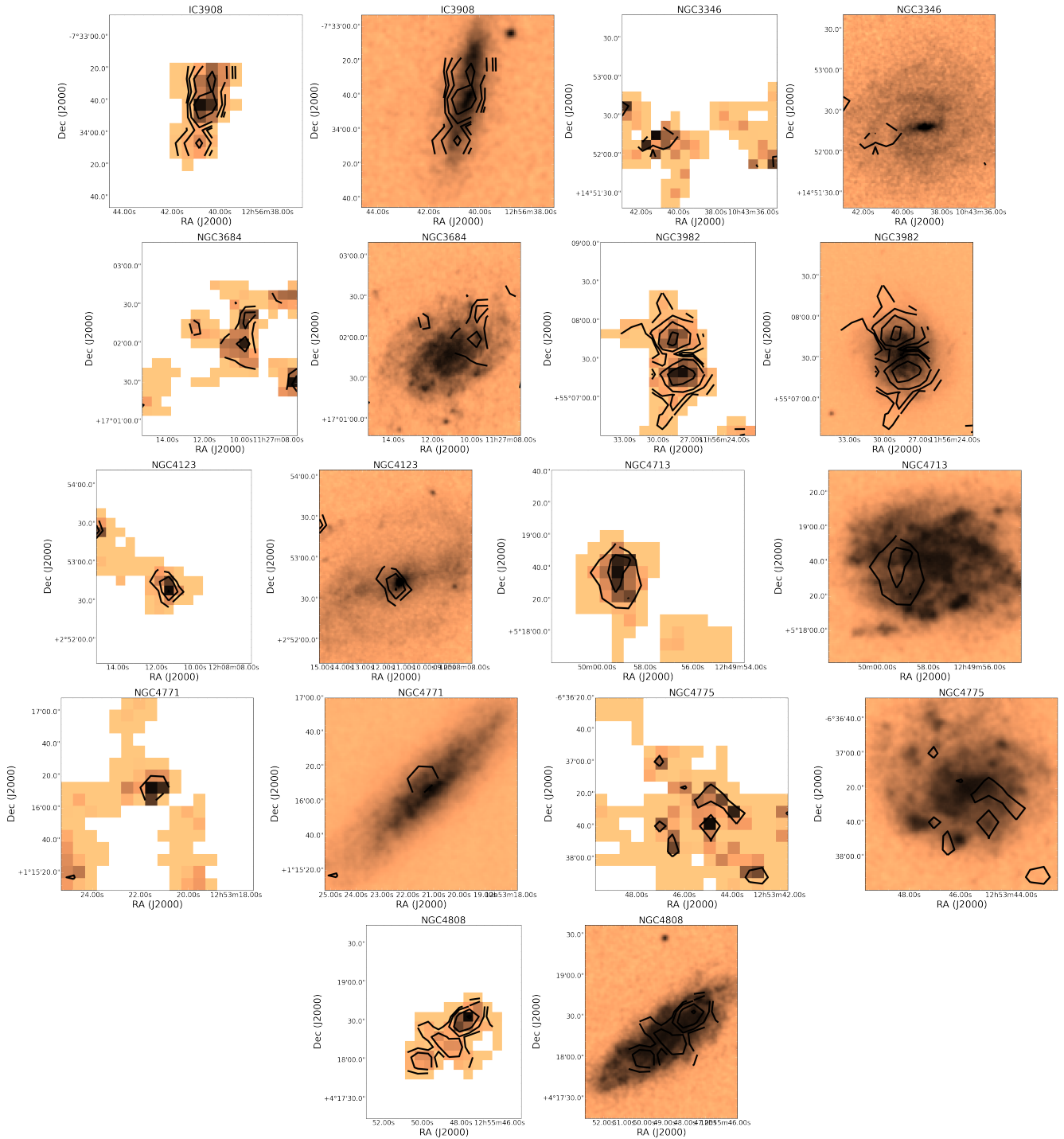


Figure C3. Additional images of the CO detected galaxies in the group sample. The first panel in each pair is the CO $J = 3 - 2$ integrated galaxy map with black contour levels overlaid at 0.5, 1, 2, 4, 8, and 16 K km s^{-1} . The second panel is the same contour levels overlaid on the optical image from the Digitized Sky Survey.

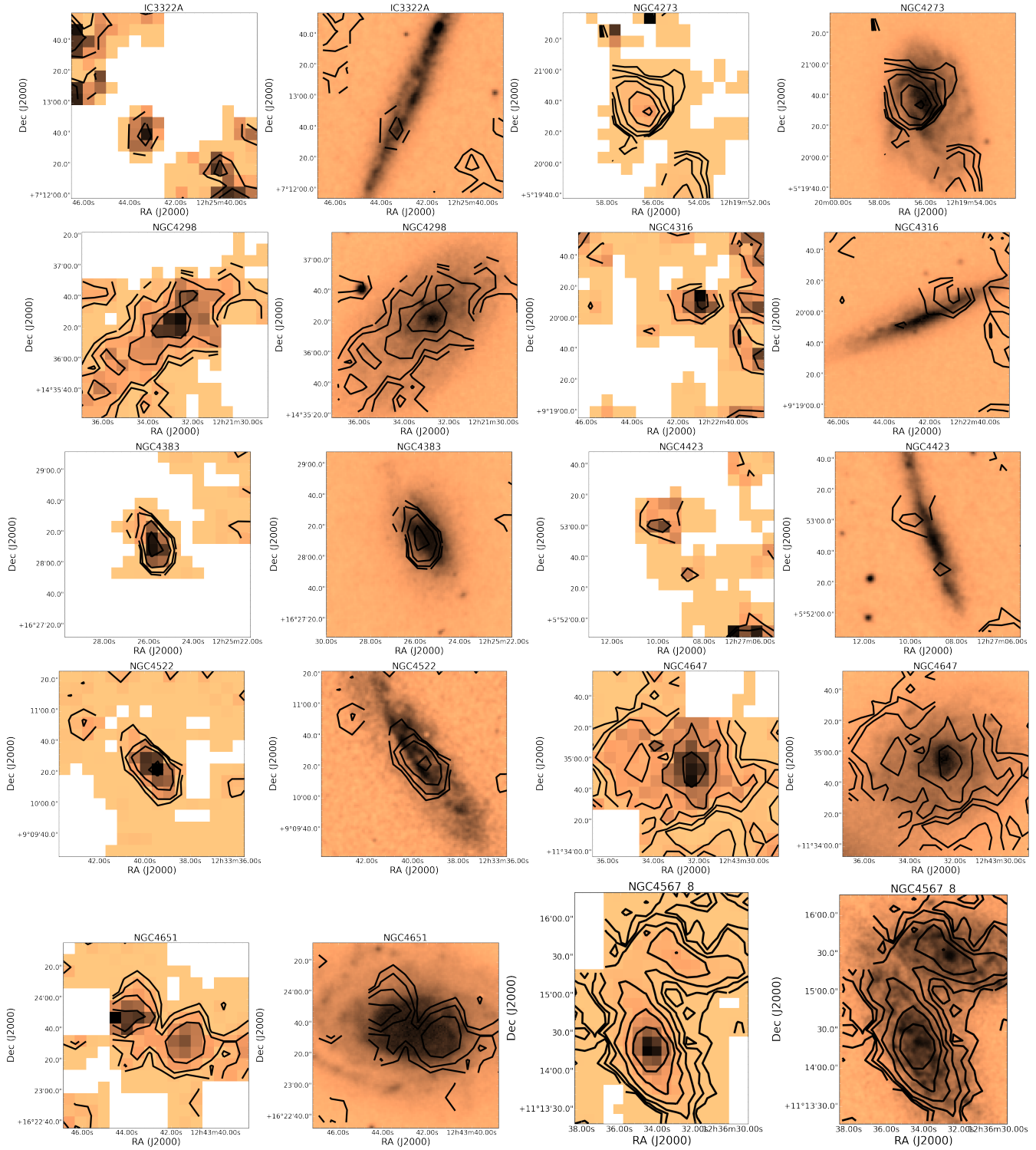


Figure C4. Images of the CO detected galaxies in the Virgo sample. The first panel in each pair is the CO $J = 3 - 2$ integrated galaxy map with black contour levels overlaid at 0.5, 1, 2, 4, 8, and 16 K km s^{-1} . The second panel is the same contour levels overlaid on the optical image from the Digitized Sky Survey. Note that NGC 4567 and 4568 were combined into one image due to their close proximity.

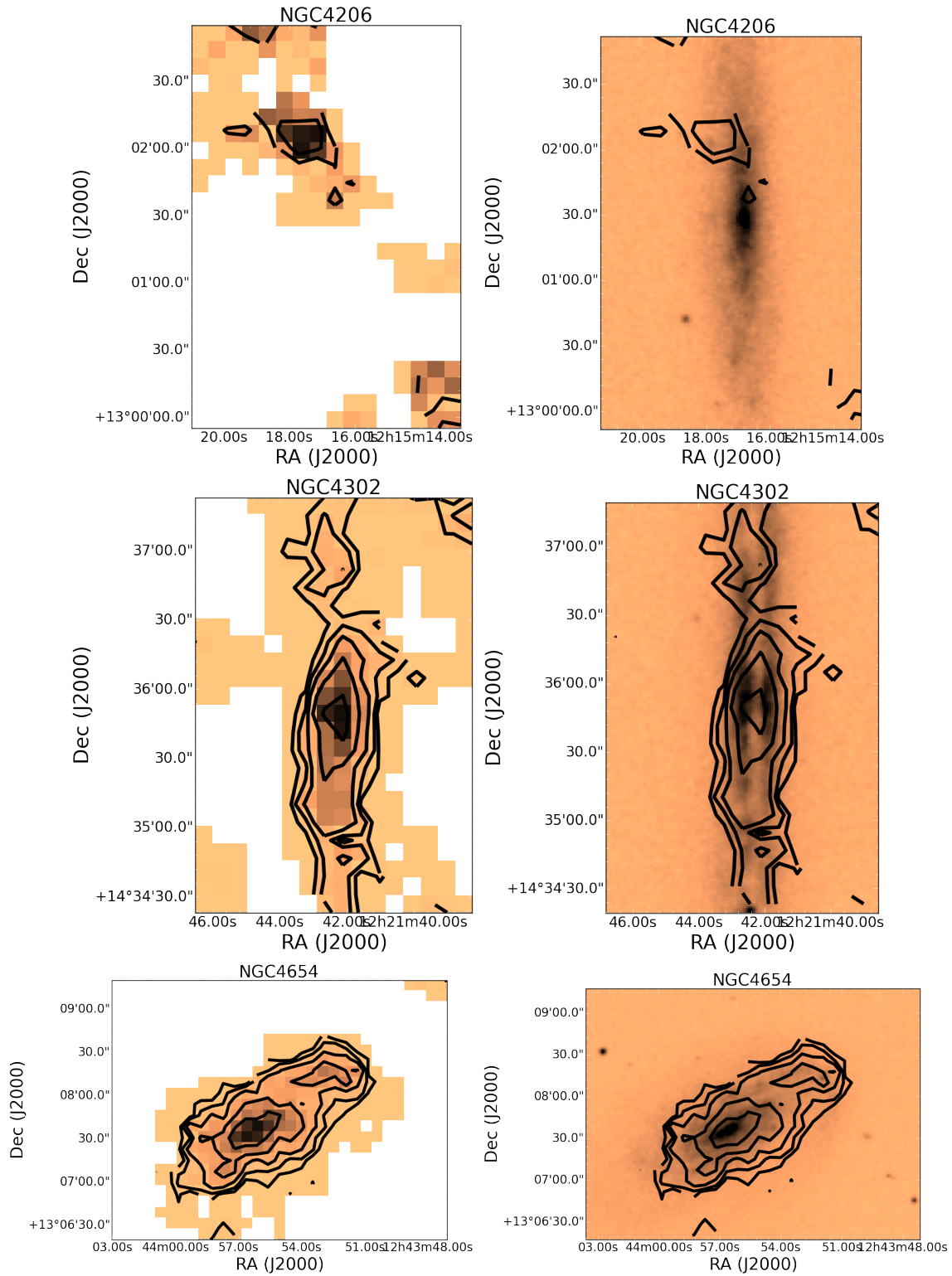


Figure C5. Images of the CO detected galaxies in the Virgo sample, observed with two overlapping fields. The first panel in each pair is the CO $J = 3 - 2$ integrated galaxy map with black contour levels overlaid at 0.5, 1, 2, 4, and 16 K km s^{-1} . The second panel is the same contour levels overlaid on the optical image from the Digitized Sky Survey.

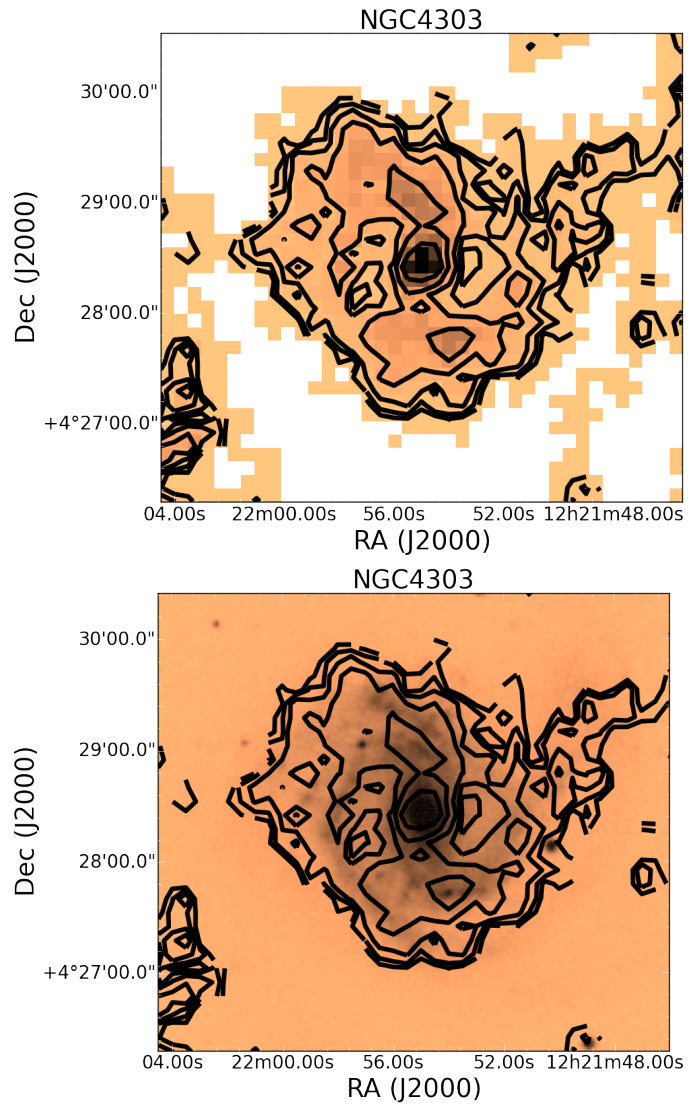


Figure C6. Images of NGC 4303 in the Virgo sample, observed using the raster method. The first panel in each pair is the CO $J = 3 - 2$ integrated galaxy map with black contour levels overlaid at 0.5, 1, 2, 4, 8, and 16 K km s^{-1} . The second panel is the same contour levels overlaid on the optical image from the Digitized Sky Survey.